Applied Catalysis B: Environmental 269 (2020) 118847

Contents lists available at ScienceDirect

Applied Catalysis B: Environmental

journal homepage: www.elsevier.com/locate/apcatb

Crystal facet dependence of carbon chain growth mechanism over the Hcp and Fcc Co catalysts in the Fischer-Tropsch synthesis

Riguang Zhang[a], Li Kang[a], Hongxia Liu[a], Baojun Wang[a,*], Debao Li[b], Maohong Fan[c,d,**]

[a] Key Laboratory of Coal Science and Technology of Ministry of Education and Shanxi Province, Taiyuan University of Technology, Taiyuan 030024, Shanxi, PR China
[b] State Key Laboratory of Coal Conversion, Institute of Coal Chemistry, Chinese Academy of Science, Taiyuan 030001, Shanxi, PR China
[c] College of Engineering and Applied Science, and School of Energy Resources Engineering, University of Wyoming, Laramie, WY, 82071, USA
[d] School of Civil and Environmental Engineering, Georgia Institute of Technology, Atlanta, GA, 30332, USA

ARTICLE INFO

Keywords:
Fischer-Tropsch synthesis
Co catalysts
Crystal facet
Carbon chain growth
Density functional theory

ABSTRACT

Revealing the sensitivity of Co crystal facet structure to the mechanism of carbon chain growth in the Fischer-Tropsch synthesis (FTS) is of great importance yet challenging issue in the heterogeneous catalysis. According to the occupied proportion of different crystal facets in the hcp and fcc Co crystal phases, this study for the first time identifies the essential relationship between the performance of carbon chain growth in the FTS and the structure of Co crystal facets. The hcp Co generally presents much higher intrinsic activity for the carbon chain growth *via* the carbide mechanism compared to the fcc Co *via* the CHO insertion mechanism. The findings will deepen our understandings about the crystal facet structure-dependent performances of Co catalysts in the FTS reactions, and provides a clear clue for the preparation of high performance Co catalysts through the rational design of Co crystal facet with more stepped B_5-type active unit.

1. Introduction

Fischer-Tropsch synthesis (FTS) [1–4] provides alternative non-petroleum route to liquid hydrocarbon fuel synthesis by the direct syngas (CO and H_2) conversion. Co-based catalysts are extensively used in FTS due to the excellent performance for linear hydrocarbons formation and poor activity for water-gas shift (WGS) reaction compared to Fe-based catalysts [5–7]. For FTS reactions on the Co-based catalysts, both carbide mechanism and CO/CHO insertion mechanism are generally recognized [8–12]. Our recent density functional theory (DFT) studies [13,14] fully investigated the growth mechanism of carbon chain on the Co(10-10) and (10–11) facets, indicating that carbide mechanism mainly contribute to carbon chain growth *via* RCH_2 coupling with CH_2. Whereas, Masters et al. [15] elucidated that CO activation and hydrogenation can produce CH_x species, then, CO insertion into CH_x can form CH_xCO and subsequently take part in the C—O bond cleavage to produce C_2H_x intermediates, further follow the similar cycle reactions to realize carbon chain growth. Pichler and Schulz et al. [16] originally proposed the CO insertion mechanism that RCH_2CO can produced through CO insertion into RCH_2; further, Zhuo et al. [17] found that the C—O bond scission of RCH_2CO can realized the carbon chain formation on the Co(0001) surface, however, CO insertion into RCH_2 occurred difficultly. Alternatively, CHO insertion mechanism was also proposed, for instance, the theoretical researches by Zhao et al. [12] clarified that the carbon chain formation on the Co(0001) facet is mainly attribute to CHO insertion into CH_x rather than CO insertion into CH_x; Chen et al. [18] believed that CHO insertion mechanism was more reasonable for the carbon chain formation on the flatted Co(111) facet, moreover, CHO formation was facilitated on the stepped Co(111) facet; Xu et al. [19] reported that CHO insertion into CH_x to CH_xCHO is also facilitated by introducing Cu into Co.

In the process of FTS reactions, the continuous hydrogenation of CH_x species can produce methane to decrease the production of long-chain hydrocarbons *via* the CH_x coupling. Previous studies showed that methane formation goes through the successive hydrogenation of CH that is from direct dissociation of HCOH on Co(0001) facet [20–22]. Gong et al. [23] found methane formation is determined by CH_3 hydrogenation on the Co(0001) facets. Further, alcohols species (typically methanol, ethanol) can be produced in the process of C_{2+} hydrocarbons formation from syngas [24,25]. Pei et al. [26] obtained high alcohols

* Corresponding author at: Key Laboratory of Coal Science and Technology of Ministry of Education and Shanxi Province, Taiyuan University of Technology, Taiyuan 030024, Shanxi, PR China.
** Corresponding author at: College of Engineering and Applied Science, and School of Energy Resources Engineering, University of Wyoming, Laramie, WY 82071, USA.
E-mail addresses: wangbaojun@tyut.edu.cn, wbj@tyut.edu.cn (B. Wang), mfan@uwyo.edu, mfan3@mail.gatech.edu (M. Fan).

https://doi.org/10.1016/j.apcatb.2020.118847
Received 5 December 2019; Received in revised form 28 February 2020; Accepted 1 March 2020
Available online 02 March 2020
0926-3373/

over Co/Co_2C catalysts with excellent activity and selectivity in FTS reactions. Wang et al. [27] clarified that the Cu-Co bimetallic catalysts simultaneously accelerate the formation of acyl intermediate and $CH_xC(H)O(x = 1 \sim 3)$, followed by its hydrogenation to form ethanol. These results show that the formation of methane and alcohols species reduce the selectivity and productivity of C_{2+} hydrocarbons in FTS reactions over Co-based catalysts, as a result, fundamentally understanding the formation mechanism of methane and alcohols species over the Co-based catalysts in the formation process of long-chain hydrocarbons can provide clue for inhibiting methane and alcohols.

For Co catalysts, both hexagonal close-packed (hcp) and face-centered cubic (fcc) crystallographic morphologies exist in the FTS reactions [28]. FTS activity over the hcp Co is higher than that over the fcc Co [29–31], however, the hcp Co can be transformed to the fcc Co above 690 K [32], moreover, the fcc Co is more stable than the hcp Co as the particle size is less than 100 nm [33,34]. Liu et al. [29] found that CO activation presented strong sensitivity to Co crystal facet, that is, direct dissociation on the hcp Co and hydrogen-assisted dissociation on the fcc Co. Thus, it is inferred that the mechanism of carbon chain growth in the FTS reactions on Co catalysts may be also sensitive to Co crystal facet. Meanwhile, Liu et al. [29] also demonstrated that the (0001), (10-10), (11–20), (11–21), (10–12) and (10–11) were the exposed facets for the hcp Co catalysts, which occupy 18 %, 28 %, 6%, 1%, 12 % and 35 % of total surface area, respectively; for the fcc Co catalysts, the (111), (110), (311) and (100) facets occupy 70 %, 8%, 10 % and 12 % of total surface area, respectively, even the (111) facet has the highest surface area proportion in the fcc Co, but the activity of this facet is lower than the corrugated (311), (100) and (110) facets. Namely, Co(111) facet with 70 % of total surface area only can reflect most of the surface structural characteristics for fcc Co catalysts instead of the whole activity for fcc Co catalysts; however, the reactions sites on the Co(111) facet are the most abundant sites, connecting the defects.

Up to now, DFT calculations in our group [13,14,18,35] have systematically investigated the carbon chain growth mechanism over the fcc Co(111), hcp Co(0001), (10-10) and (10–11) facets, revealing that the carbon chain growth mechanism is dependent on the crystal structure of Co catalyst, for example, both Co(111) and Co(0001) facets occupying 70 % and 18 % of total surface area corresponding to the fcc and hcp Co followed the preferred CHO insertion mechanism [18,35]; whereas the carbide mechanism accomplished the carbon chain growth over the stepped Co(10-10) [13] and (10–11) [14] facets with the surface area proportion of 28 % and 35 % in the hcp Co, respectively. However, until now, no study concerning the growth mechanism of carbon chain on the Co(10–12) facet with the surface area proportion of 12 % in the hcp Co is reported. Accordingly, further effort is required for researchers to illustrate the carbon chain growth mechanism on the Co(10–12) facet, which is also very necessary to identify the facet structure-performance relationship of Co catalyst.

This study is designed to firstly investigate the growth mechanism of carbon chain in the FTS reactions on the Co(10–12) facet by DFT calculations and microkinetic modeling, correspondingly, the influences of methane and alcohols on C_{2+} hydrocarbons formation are identified. More importantly, based on the information of Co(10–12) facet, among the mostly exposed hcp Co(10–12), (0001) [35], (10-10) [13], (10–11) [14] and fcc Co(111) [18] facets, the comparisons about the carbon chain growth mechanism of FTS reactions together with the effects of methane and alcohols species are carried out, which is expected to obtain the structure-performance relationship for FTS reactions on the Co catalysts. The findings will provide a clear clue for the preparation of high performance catalysts through the rational regulation of Co crystal facet with maximum mass-specific reactivity.

2. Computational methods and models

All of the plane-wave-based DFT calculations were implemented by the Vienna Ab Initio Simulation Package (VASP) code [36,37], and the projector augmented wave (PAW) method have been employed. The generalized gradient approximation (GGA) with Perdew-Burke-Ernzerhof (PBE) [38] was used for the exchange correlation function. The spin-polarized effect was considered in our calculations due to the magnetic properties of metal Co. The kinetic cut off energy for describing the electronic wave functions was set to 400 eV. A $5 \times 5 \times 1$ Monkhorst − Pack *k*-point grid was used [39]. Structure optimizations were performed until the total energies were converged to 5×10^{-6} eV and the forces acting on the relaxed ions were less than 0.03 eV/Å. The climbing-image nudged elastic band (CI-NEB) method [40,41] was employed to search the transition states (TS), then, the dimer method was used to optimize the located TS [42,43]. Moreover, the only one imaginary frequency corresponding to the TS structure is confirmed. Further, since the temperature of realistic FTS conditions [44,45] is 473 ~ 623 K, the values of all energies in this study are obtained at 500 K (see details in the Supplementary Material).

The Co(10–12) facet was modeled by a nine-layer $p(3 \times 2)$ supercell, resulting from the optimized hcp Co bulk with the lattice constants of a = b = 2.489 Å, c = 4.029 Å (the experimental value of a = b = 2.51 Å, c = 4.10 Å [46]). Repeating slabs were separated by a vacuum distance of 15 Å to prevent noticeable interaction in the Z direction. In addition, the adsorption free energies and the corresponding adsorption configurations of C_4 species ($CH_3CH_2CH_2CH_2$, C_4H_{10} and $CH_3CH_2CH_2CHO$) are calculated in a 20 Å vacuum spacing to test the rationality of a 15 Å vacuum spacing, as listed in Table S1, the results show that the differences of adsorption free energies and adsorption configurations between two surface models with 15 and 20 Å vacuum spacing are negligible. Namely, the obtained results confirm that a 15 Å vacuum spacing used in this study is large enough to neglect the interactions between the repeating slabs. Further, the dipole correction is not applied in this work, firstly, a large number of studies [47–50] have investigated FTS reactions over Co catalysts without considering the effect of the dipole on reaction mechanism, and the corresponding results can well clarify the reaction mechanism, which agrees with the experiment; moreover, the adsorption free energies and stable adsorption configurations of C_4 species ($CH_3CH_2CH_2CH_2$, C_4H_{10} and $CH_3CH_2CH_2CHO$) are re-calculated with the application of dipole corrections, as listed in Table S1, suggesting that the adsorption free energies of C_4 species are reduced by only 1.5 kJ·mol^{-1} after including dipole corrections, and there is negligible change in the adsorption configurations. The bottom three layers representing the bulk were frozen in all calculations. The structure and adsorption sites of hcp Co (10–12) facet is shown in Fig. 1a; the hcp (10–11), (10-10), (0001) and the fcc Co (111) facets are shown in Fig. 1b ~ e.

3. Results and discussion

Here, the adsorption behaviors of possible species along with the process of the carbon chain growth on the Co(10–12) facet were studied (see details in Fig. 2 and Table S1). The reactions related to CO activation to form CH_x, the formations of methane, methanol, C_{2+} oxygenates and C_{2+} hydrocarbons are listed in Table 1 (see details in the Supplementary Material). Meanwhile, among the mostly exposed hcp Co(10–12), (0001) [35], (10-10) [13], (10–11) [14] and fcc Co(111) [18] facets, the comparisons about the carbon chain growth mechanism of FTS reactions together with the effects of methane and alcohols species are carried out to obtain the structure-performance relationship for the carbon chain growth of FTS reactions on the Co catalysts.

3.1. CO activation to produce $CH_x(x = 1 \sim 3)$ species

3.1.1. CO initial activation

Starting from CO + H species, as shown in Fig. 3, CO direct dissociation to CH (CO + H→C + O + H→CH + O) has the overall energy barrier of 143.5 kJ·mol^{-1}. CO hydrogenation to CHO is much easier in kinetics compared to COH formation (90.0 ***vs.*** 157.8 kJ·mol^{-1}),

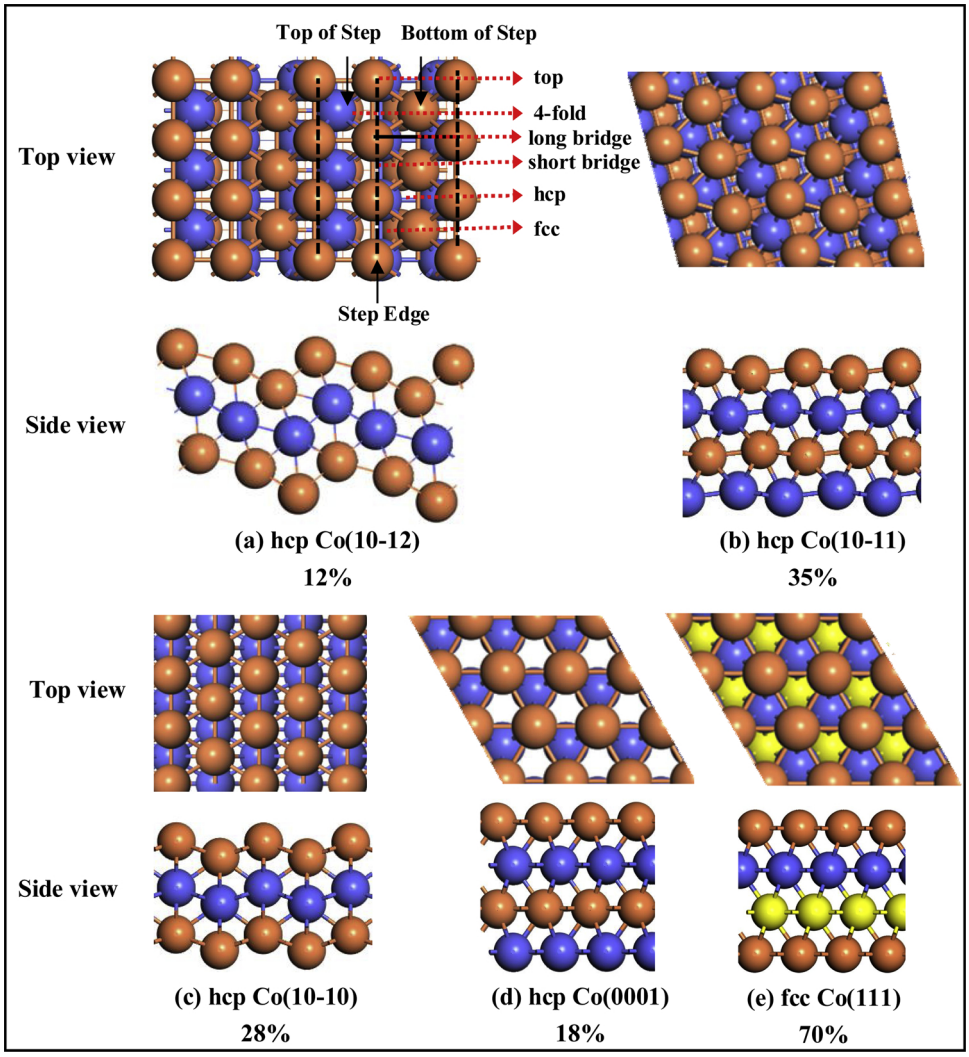

Fig. 1. The surface morphology and the corresponding proportion of the hcp (a) (10-12), (b) (10-11), (c) (10-10), (d) (0001) and (e) the fcc Co (111) facets. The percentages correspond to the relative abundance of these facets in the hcp or fcc crystal phase, respectively.

subsequently, CH formation *via* the cleavage of C—O bond in CHO (CO + H→CHO→CH + O) has the overall energy barrier of 163.3 kJ·mol^{-1}. Alternatively, the C—O bond breakage of COH can form OH and C, then, CH can be formed *via* C hydrogenation (CO + H→COH + H→C + OH + H→CH + OH) with the overall energy barrier of 157.8 kJ·mol^{-1}. Thus, compared to CO hydrogen-assisted dissociation, CO direct dissociation is thermodynamically and dynamically favored for CH formation on the Co(10–12).

The comparisons of CO initial activation mechanism among the exposed facets of hcp and fcc Co indicated that CO hydrogen-assisted dissociation *via* CHO intermediate is pronounced as the major mechanism on the hcp Co(0001) [35], (10-10) [29,51] and fcc Co(111) [18,29] facets compared to CO direct dissociation (189.4, 144.3, 177.0 ***vs.*** 230.1, 188.9, 231.4 kJ·mol^{-1}). In contrast, CO hydrogen-assisted dissociation is unlikely to occur, CO direct dissociation is more conducive on the hcp Co(10–11) [29,51], (11–21) [29] and (10–12) [29] facets (163.6, 138.9, 134.1 ***vs.*** 143.7, 103.2, 129.3 kJ·mol^{-1}).

3.1.2. The production of CHx(x = 1 ~ 3) intermediates

Based on CO initial activation to produce CH, CH is preferentially hydrogenated to produce CH_2 in kinetics (60.1 kJ·mol^{-1}), however, CH_2 is incline to undergo the dehydrogenation to produce CH in kinetics instead of its hydrogenation to CH_3 (7.4 ***vs.*** 68.5 kJ·mol^{-1}), thus, the dominant CH_x species is CH monomer. Meanwhile, the C—O bond breakage of CH_xO(x = 1 ~ 3) to produce CH_x(x = 1 ~ 3) species (163.3, 200.4 and 216.3 kJ·mol^{-1}) is kinetically difficult compared to CO direct dissociation and hydrogenation to produce CH_x(x = 1 ~ 3) species (143.5 kJ·mol^{-1}).

Above results show that CO direct dissociation dominantly contribute to CO initial activation on the Co(10–12) facet *via* the route of CO + xH→C + O + xH→CH_x + O, CH is the favored CH_x monomer. Interestingly, previous studies also found that CH species is the favored CH_x(x = 1 ~ 3) monomer arising from CO direct dissociation on the hcp Co(10–11) facet [51]. However, both CH and CH_2 species are the favored CH_x(x = 1 ~ 3) monomer produced by CO hydrogen-assisted dissociation mechanism on the hcp Co(0001) [35] and fcc Co(111) facets [18]; that is CH_2 species on the hcp Co(10-10) produced by CO hydrogen-assisted dissociation *via* CH_2O intermediate [51]. Thus, the existence form of favored CH_x(x = 1 ~ 3) monomer and its preferential formation route strongly depend on the crystal facet of Co catalyst.

3.1.3. The production of methane and methanol, and their effects on CH_x formation

Starting from CO + H species (see Fig. 3), methane formation (black line) affects the amount of CH_x species to take part in carbon chain growth due to the same overall energy barrier of 143.5 kJ·mol^{-1}. However, the C—O bond cleavage of CH_xO to produce CH_x(x = 2, 3) are dynamically favorable than CH_xO hydrogenation to methanol (red line)

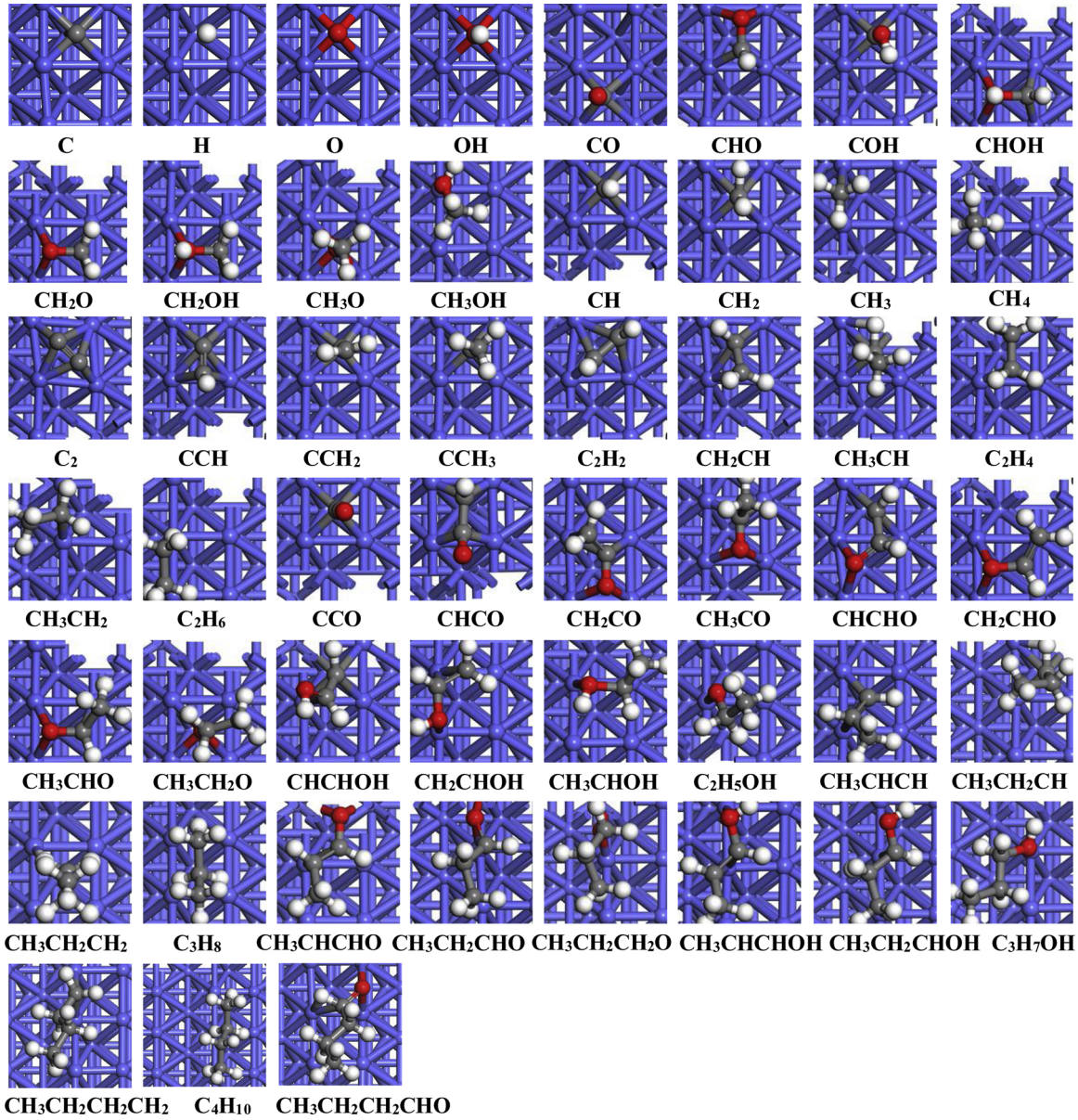

Fig. 2. The most stable adsorption structures of all possible species involved in C_4H_{10} formation from syngas on the Co(10-12) facet.

(230.2 kJ·mol^{-1}), implying that the effect of methanol on CH_x formation is negligible. Namely, the Co(10–12) facet exhibits higher activity and selectivity toward $CH_x(x = 1 \sim 3)$ and methane instead of methanol.

Identical conclusions were illustrated in the previous studies that $CH_x(x = 1 \sim 3)$ formation is more kinetically favored (132.3, 153.7, 189.4 and 177.0 kJ·mol^{-1}) than methanol (189.8, 228.7, 257.7 and 228.1 kJ·mol^{-1}) on the hcp Co(10-10) [13], (10–11) [14], (0001) [35] and fcc Co(111) facets [18], respectively. However, methane formation probably decrease the selectivity and production of $CH_x(x = 1 \sim 3)$ due to the close energy barrier on the hcp Co(10-10) [13], (10–11) [14], (0001) [35] and fcc Co(111) facets [18] (132.3, 153.7, 189.4, 177.0 ***vs.*** 132.3, 171.0, 179.0, 167.2 kJ·mol^{-1}). Accordingly, it is concluded that 81 % hcp and 70 % fcc Co crystal facets effectively inhibit methanol formation, but methane affect the selectivity of CH_x.

3.2. The carbon chain growth starting from $CH_x(x = 1 \sim 3)$ species

3.2.1. The carbon chain initiation

When $CH_x(x = 1 \sim 3)$ species is formed, the carbon chain initiation can be realized by $CH_x(x = 0 \sim 3)$ species reacting with CH_x or CO to C_2H_y or CH_xCO, respectively. Meanwhile, CO hydrogenation to CHO is much easier in kinetics than CO direct dissociation (90.0 ***vs.*** 143.5 kJ·mol^{-1}), moreover, the hydrogen-rich atmosphere for FTS reactions can promote CHO formation, which is in favor of carbon chain initiation formation [17]. In this work, the $CH_x(x = 0 \sim 3)$-related reactions (coupling, CHO/CO insertion and hydrogenation) are examined on the Co(10–12) facet (see details in the Supplementary Material).

For the C-related reactions (Fig. 4a), C is preferentially hydrogenated to CH in kinetics (71.2 kJ·mol^{-1}) compared to its coupling and insertion reactions; thus, Co(10–12) effectively suppress C deposition and promote surface C hydrogenation to produce CH. For the CH-related reactions (Fig. 4b), CH hydrogenation to CH_2 is the most favorable (60.1 kJ·mol^{-1}); in addition, CH coupling with CH/CH_2 to C_2H_2/$CHCH_2$ are competitive in kinetics with CHO/CO reaction with CH to CHCHO/CHCO (93.5/98.6 ***vs.*** 91.2/95.3 kJ·mol^{-1}). For the CH_2-related reactions (Fig. 4c), CH_2 prefers to undergo self-coupling to C_2H_4 (56.1 kJ·mol^{-1}). For the CH_3-related reactions (Fig. 4d), CH_3 is incline to be hydrogenated to methane (46.1 kJ·mol^{-1}), which is much easier in kinetics than CH_3 dissociation into CH_2 (75.9 kJ·mol^{-1}); in addition,

Table 1
All possible elementary reactions involving in C_4H_{10} formation with the corresponding activation energy barriers (G_a), reaction energies (ΔG), rate constants (k) and the imaginary frequency (ν) of transition state at 500 K on the Co(10-12) facet.

Reactions		ν (cm^{-1})	$G_a(E_a)$ ($kJ \cdot mol^{-1}$)	$\Delta G(\Delta E)$ ($kJ \cdot mol^{-1}$)	k (s^{-1})
R1	CO→C + O	415*i*	143.5(151.0)	−12.1(−21.2)	0.11×10^{-3}
R2	CO + H→CHO	683*i*	90.0(85.0)	53.5(46.6)	1.20×10^{3}
R3	CO + H→COH	1457*i*	157.8(155.0)	72.0(71.6)	0.16×10^{-4}
R4	CHO→CH + O	448*i*	109.8(110.5)	−47.2(−54.8)	0.41×10^{2}
R5	COH→C + OH	337*i*	82.7(88.8)	−57.6(−3.2)	3.86×10^{4}
R6	CHO + H→CHOH	1273*i*	172.0(171.9)	112.1(114.6)	1.06×10^{-5}
R7	CHOH→CH + OH	198*i*	56.0(64.2)	−140.3(−139.6)	1.03×10^{8}
R8	CHO + H→CH_2O	798*i*	59.2(58.1)	22.1(24.1)	5.07×10^{6}
R9	CH_2O + H→CH_2OH	1238*i*	154.5(155.3)	84.1(88.7)	0.90×10^{-3}
R10	CH_2OH + H→CH_3OH	1200*i*	148.7(150.1)	−22.3(0)	0.42×10^{-2}
R11	CH_2O→CH_2 + O	431*i*	124.8(137.9)	−32.4(−33.2)	0.22×10^{2}
R12	CH_2O + H→CH_3O	810*i*	140.7(146.9)	11.1(21.9)	0.94×10^{-1}
R13	CH_3O→CH_3 + O	583*i*	119.1(115.2)	−64.7(−67.5)	$1.43 \times 10^{\circ}$
R14	CH_3O + H→CH_3OH	1170*i*	143.5(144.5)	57.7(71.9)	0.12×10^{-1}
R15	C + H→CH	773*i*	71.2(70.5)	13.1(13.3)	3.20×10^{5}
R16	CH + H→CH_2	784*i*	60.1(58.8)	52.7(49.9)	3.89×10^{6}
R17	CH_2 + H→CH_3	769*i*	68.5(68.4)	−7.4(−0.7)	7.18×10^{5}
R18	CH_3 + H→CH_4	194*i*	46.1(46.1)	14.8(18.5)	3.04×10^{8}
R19	C + C→C_2	194*i*	142.7(146.9)	113.3(117.1)	0.36×10^{-1}
R20	C + CH→CCH	277*i*	100.4(102.5)	32.3(35.4)	5.46×10^{2}
R21	C + CH_2→CCH_2	415*i*	116.7(116.9)	4.2(9.7)	0.70×10^{1}
R22	C + CH_3→CCH_3	336*i*	105.7(108.2)	7.9(10.1)	1.68×10^{2}
R23	C + CO→CCO	431*i*	91.6(92.9)	38.9(44.6)	3.82×10^{3}
R24	C + CHO→CCHO	—	—	—	—
R25	CH + CH→C_2H_2	450*i*	93.5(94.8)	20.0(22.9)	2.42×10^{3}
R26	CH + CH_2→CH_2CH	453*i*	98.6(99.8)	29.0(31.8)	6.98×10^{2}
R27	CH + CH_3→CH_3CH	438*i*	147.2(152.2)	37.2(38.2)	0.14×10^{-1}
R28	CH + CO→CHCO	320*i*	95.3(91.8)	84.9(86.4)	4.91×10^{2}
R29	CH + CHO→CHCHO	395*i*	91.2(93.6)	49.3(52.8)	5.51×10^{3}
R30	CH_2 + CH_2→C_2H_4	309*i*	56.1(62.0)	−24.9(−21.2)	3.77×10^{9}
R31	CH_2 + CH_3→CH_3CH_2	438*i*	100.1(101.2)	−7.5(−2.8)	4.63×10^{2}
R32	CH_2 + CO→CH_2CO	439*i*	159.6(145.5)	29.2(23.2)	7.29×10^{-6}
R33	CH_2 + CHO→CH_2CHO	442*i*	70.0(73.3)	−29.2(−27.5)	1.13×10^{6}
R34	CH_3 + CH_3→C_2H_6	581*i*	152.1(153.8)	−41.8(−16.4)	0.02×10^{-1}
R35	CH_3 + CO→CH_3CO	669*i*	104.5(127.7)	38.5(30.1)	3.33×10^{4}
R36	CH_3 + CHO→CH_3CHO	227*i*	242.6(251.3)	2.3(1.4)	1.11×10^{-12}
R37	C_2H_2 + H→CH_2CH	485*i*	76.6(63.0)	48.9(49.8)	3.93×10^{3}
R38	CH_2CH + H→CH_3CH	881*i*	30.0(27.8)	−21.4(−11.8)	4.38×10^{9}
R39	CH_2CH + H→C_2H_4	330*i*	56.9(43.9)	−27.6(−27.1)	5.08×10^{5}
R40	C_2H_4 + H→CH_3CH_2	818*i*	77.8(74.0)	−17.5(−12.6)	3.10×10^{4}
R41	CH_3CH + H→CH_3CH_2	900*i*	55.5(54.1)	−3.2(−2.5)	1.16×10^{7}
R42	CH_3CH_2 + H→C_2H_6	820*i*	67.5(75.7)	−15.1(−4.9)	6.70×10^{6}
R43	CHCHO→C_2H_2 + O	392*i*	68.7(66.3)	−55.1(−53.9)	3.83×10^{5}
R44	CHCHO + H→CHCHOH	1333*i*	55.7(55.5)	53.5(59.9)	1.48×10^{7}
R45	CHCHO + H→CH_2CHO	860*i*	18.5(20.0)	−3.1(−4.8)	1.77×10^{11}
R46	CH_2CHO→CH_2CH + O	431*i*	125.9(122.5)	13.2(12.8)	$0.32 \times 10^{\circ}$
R47	CH_2CHO + H→CH_2CHOH	1112*i*	152.0(146.2)	80.8(95.8)	0.30×10^{-3}
R48	CH_2CHO + H→CH_3CHO	785*i*	48.3(45.9)	8.8(14.6)	5.28×10^{7}
R49	CH_3CHO→CH_3CH + O	330*i*	174.7(171.7)	−9.5(−4.2)	2.88×10^{-6}
R50	CH_3CHO + H→CH_3CHOH	1160*i*	115.5(116.6)	103.2(108.2)	1.15×10^{1}
R51	CH_3CHO + H→CH_3CH_2O	825*i*	82.6(92.6)	−3.8(10.3)	2.64×10^{5}
R52	CH_3CH_2O→CH_3CH_2 + O	488*i*	134.5(128.3)	4.8(−2.7)	$8.09 \times 10^{\circ}$
R53	CH_3CH_2O + H→C_2H_5OH	1210*i*	116.8(113.5)	59.0(-38.2)	$5.28 \times 10^{\circ}$
R54	CH_3CH + CH→CH_3CHCH	401*i*	163.7(160.9)	−22.7(−30.6)	4.12×10^{-5}
R55	CH_3CH_2 + CH→CH_3CH_2CH	380*i*	94.7(114.5)	30.1(27.1)	3.63×10^{4}
R56	CH_3CH_2 + CH_2→$CH_3CH_2CH_2$	278*i*	61.4(52.1)	−19.5(−30.7)	1.79×10^{7}
R57	CH_3CH_2CH + H→$CH_3CH_2CH_2$	801*i*	83.2(66.8)	15.2(18.3)	5.79×10^{4}
R58	$CH_3CH_2CH_2$ + H→C_3H_8	766*i*	72.8(50.1)	14.8(20.2)	6.97×10^{5}
R59	CH_3CH + CHO→CH_3CHCHO	488*i*	84.5(48.3)	−57.1(−78.1)	4.20×10^{4}
R60	CH_3CH_2 + CHO→CH_3CH_2CHO	444*i*	93.5(77.7)	−9.5(−12.8)	4.82×10^{3}
R61	CH_3CHCHO→CH_3CHCH + O	355*i*	107.4(111.9)	23.1(30.7)	1.69×10^{2}
R62	CH_3CHCHO + H→$CH_3CHCHOH$	1123*i*	143.2(144.3)	56.3(49.6)	$0.18 \times 10^{\circ}$
R63	CH_3CHCHO + H→CH_3CH_2CHO	800*i*	80.0(74.8)	12.2(5.6)	7.55×10^{5}
R64	CH_3CH_2CHO→CH_3CH_2CH + O	200*i*	79.8(79.4)	−33.2(−12.5)	9.83×10^{5}
R65	CH_3CH_2CHO + H→CH_3CH_2CHOH	1088*i*	144.9(155.6)	53.6(42.8)	$6.48 \times 10^{\circ}$
R66	CH_3CH_2CHO + H→$CH_3CH_2CH_2O$	799*i*	118.5(134.6)	−25.6(35.4)	1.14×10^{2}
R67	$CH_3CH_2CH_2O$→$CH_3CH_2CH_2$ + O	456*i*	118.6(125.4)	−27.7(−26.4)	1.66×10^{1}
R68	$CH_3CH_2CH_2O$ + H→C_3H_7OH	1056*i*	192.9(162.3)	95.6(63.2)	1.98×10^{-7}
R69	$CH_3CH_2CH_2$ + CH_2→$CH_3CH_2CH_2CH_2$	200*i*	24.9(28.5)	−37.6(−44.9)	7.07×10^{10}
R70	$CH_3CH_2CH_2CH_2$ + H→C_4H_{10}	671*i*	72.2(64.2)	−19.6(−14.4)	1.37×10^{2}
R71	$CH_3CH_2CH_2$ + CHO→$CH_3CH_2CH_2CHO$	290*i*	80.5(75.6)	1.9(-2.5)	1.11×10^{5}

*It is noted that the values in the parentheses is at 0 K. "—" mean that the reaction does not exist.

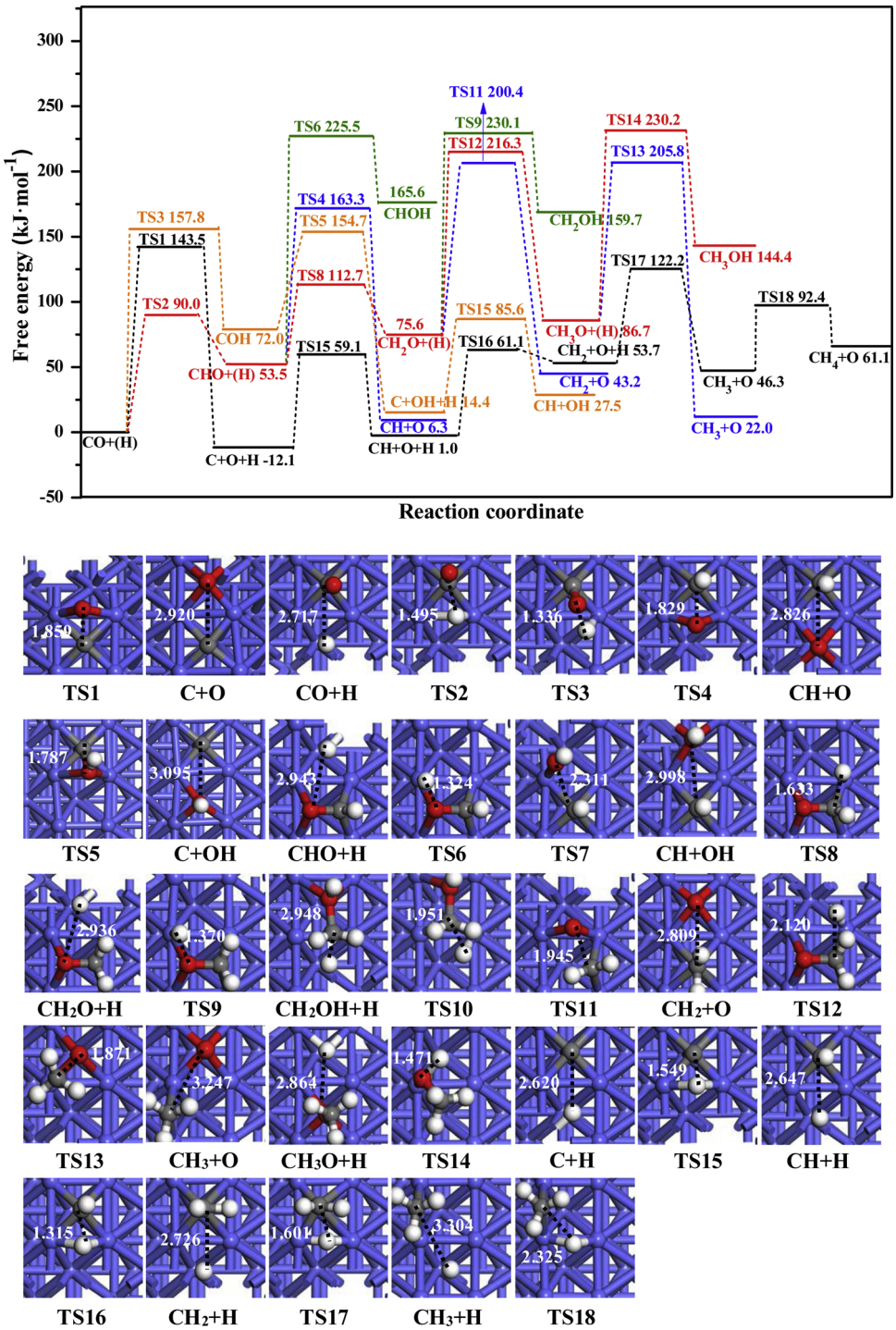

Fig. 3. The free energy profile of CO activation to CH_x(x = 1-3), CH_4 and CH_3OH formation at 500 K together with the structures of initial states (ISs), transition states (TSs) and final states (FSs) on the Co(10-12) facet. Bond lengths are in Å.

CH_3 hardly undergoes self-coupling and CHO/CO insertion leading to C_2H_6 and CH_3CHO/CH_3CO (152.1 and 242.6/104.5 kJ·mol^{-1}). Thus, both CH and CH_2 as the abundant CH_x species, produced by C hydrogenation, are responsible for the carbon chain initiation by the coupling and self-coupling between CH and CH_2 species to form $CHCH_2$, C_2H_2 and C_2H_4, as well as that by CHO/CO insertion into CH to CHCHO/CHCO. Meanwhile, CHO insertion into CH_x is more favorable than CO insertion into CH_x, which agrees with the observation from the previous studies [12,18,35]. Thus, the reactions related to the formation of C_2 hydrocarbons *via* the CH/CH_2 coupling or CHO insertion into CH will be examined on the Co(10–12) facet.

Similarly, on Co(10–11) facet, both CH and CH_2 produced by C hydrogenation are considered as the most abundant CH_x species [14], and the initial formation of carbon chain are accomplished *via* the self-coupling of CH or CH_2 to C_2H_2 or C_2H_4 and CHO insertion into CH to CHCHO. However, on the Co(111) [18] and (0001) [35] facets, although the most abundant CH_x species are CH and CH_2, it is mainly produced by CHO dissociation, and the carbon chain initiation formation is preferentially achieved by the insertion of CHO into CH or CH_2. On Co(10-10) facet [13], CH, CH_2 and CH_3 species produced by C hydrogenation are all abundant CH_x species, while the formation of initial carbon chain is realized by the self-coupling of CH_2 and the insertion of

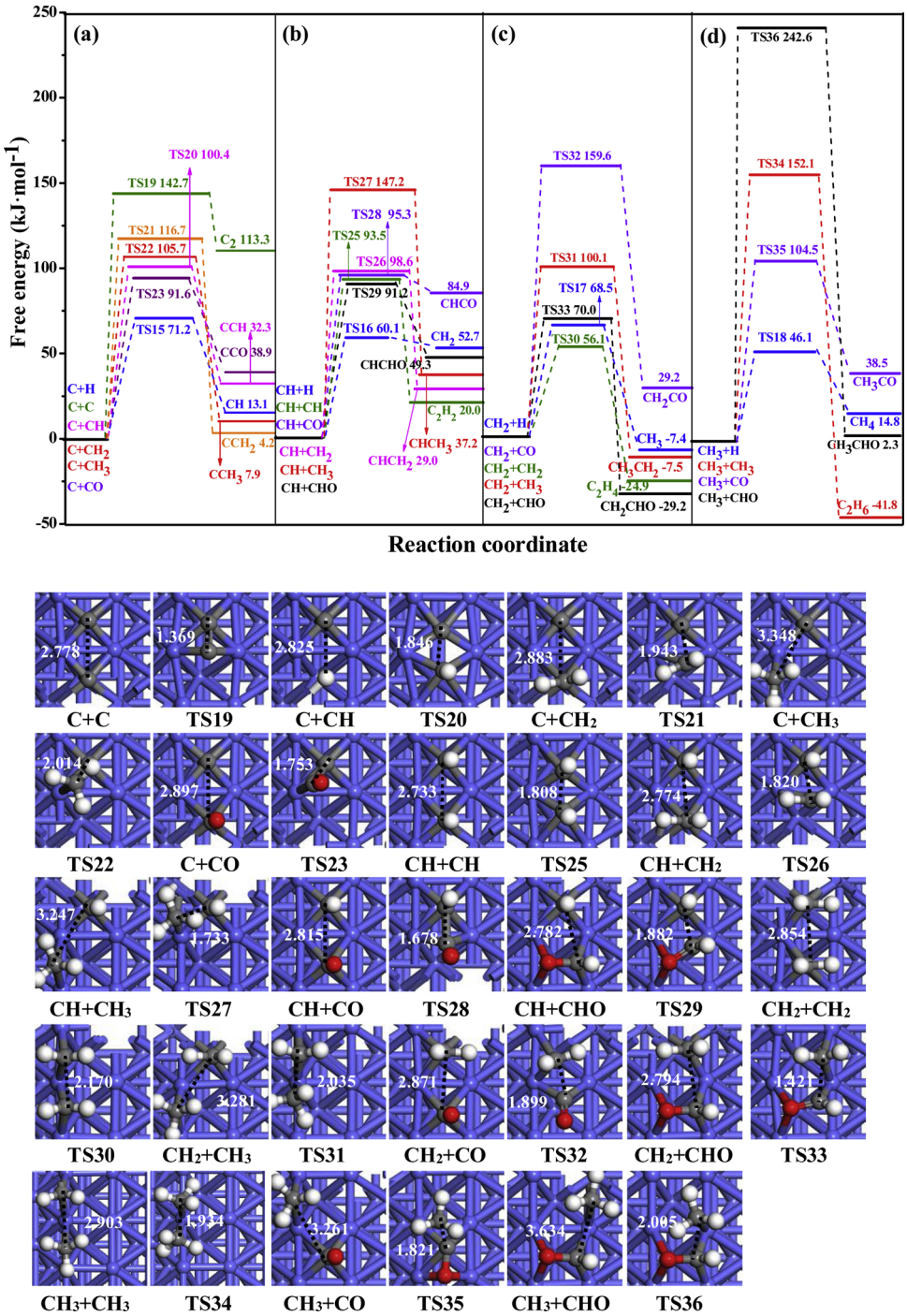

Fig. 4. The free energy profile of the reactions related to CH_x(x = 0-3) species (a) C, (b) CH, (c) CH_2, (d) CH_3 at 500 K together with the structures of initial states (ISs), transition states (TSs) and final states (FSs) on the Co(10-12) facet. Bond lengths are in Å.

CHO into CH, CH_2 or CH_3.

3.2.2. The formation of C_2 species from C_1 species

3.2.2.1. Carbide mechanism to form C_2 hydrocarbon C_2H_6 on the Co (10–12) facet. As depicted in Fig. 5, beginning with CH + CH species, C_2H_6 formation *via* CH self-coupling have two routes of CH + CH→C_2H_2 + (H)→CH_2CH + (H)→$\mathbf{C_2H_4}$ + (H)→ $\mathbf{CH_3CH_2}$ + (H)→$\mathbf{C_2H_6}$ (black line) and CH + CH→C_2H_2 + (H)→CH_2CH + (H)→ $\mathbf{CH_3CH}$ + (H)→$\mathbf{CH_3CH_2}$ + (H)→$\mathbf{C_2H_6}$ (blue line), however, the latter route *via* the CH_3CH intermediate to produce C_2H_6 is favorable in kinetics than the former route *via* the C_2H_4 intermediate (111.8 ***vs.*** 125.8 kJ·mol^{-1}). Starting with the CH + H species, C_2H_6 formation *via* CH_2 self-coupling route is CH + H→CH_2 + (CH_2)→C_2H_4 + (H)→ CH_3CH_2 + (H)→$\mathbf{C_2H_6}$ (green line) requires an overall energy barrier of 108.8 kJ·mol^{-1}. However, in the route *via* the C_2H_4 intermediate, C_2H_4 prefers to be desorption instead of its hydrogenation to produce CH_3CH_2 intermediate (32.5 ***vs.*** 77.8 kJ·mol^{-1}), thus, the route *via* the C_2H_4 intermediate is not conducive to C_2H_6 formation. Alternatively, C_2H_6 can be also formed by CH coupling with CH_2, while CH coupling with CH_2 is much difficult in kinetics compared to CH self-coupling (151.3 ***vs.*** 96.6 kJ·mol^{-1}).

Thus, on the Co(10–12) facet, in terms of carbide mechanism, only CH self-coupling *via* the CH_3CH and CH_3CH_2 intermediates dominantly contribute to C_2H_6 formation.

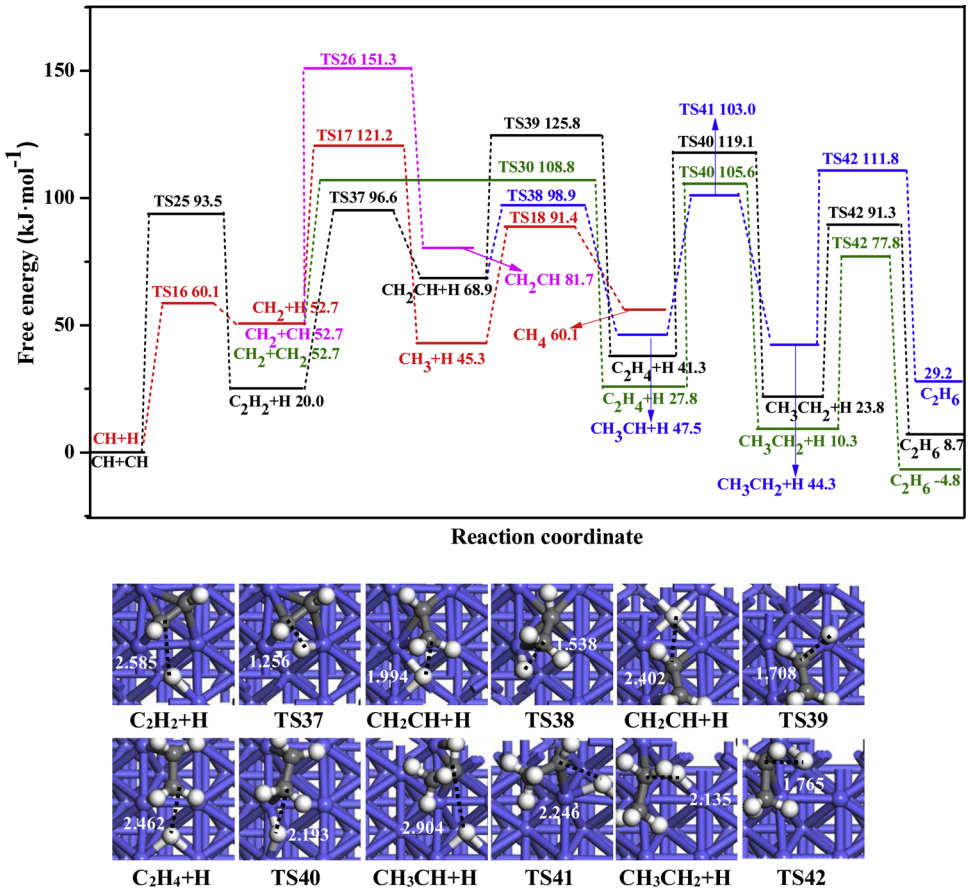

Fig. 5. The free energy profile of C_2H_6 formation with respect to CH species at 500 K together with the structures of initial states (ISs), transition states (TSs) and final states (FSs) on the Co(10-12) facet. Bond lengths are in Å.

3.2.2.2. CHO insertion mechanism to form C_2H_6 on the Co(10–12) facet. As mentioned above, CHO insertion into CH to CHCHO is easier, beginning with CHCHO species (see Fig. 6), CHCHO prefers to be hydrogenated to CH_2CHO rather than CHCHOH or its direct dissociation into CHCH + O (18.5 ***vs.*** 55.7, 68.7 kJ·mol^{-1}). Similarly, CH_2CHO successive hydrogenation to ethanol *via* the CH_3CHO and CH_3CH_2O intermediates is more favored in kinetics compared to CH_xCHO(x = 2,3) hydrogenation to CH_xCHOH, as well as their dissociation. On the other hand, starting from CHCHO species, although CHCHO hydrogenation is more favorable in kinetics than the C—O bond cleavage of CHCHO, ethanol formation by the successive hydrogenation of CHCHO is less favored in kinetics than C_2H_6 formation based on the corresponding overall energy barriers of 221.5 and 171.5 kJ·mol^{-1}, respectively. Namely, CHO insertion mechanism is favorable for C_2H_6 formation rather than ethanol, moreover, the optimal route of C_2H_6 formation *via* CHO insertion mechanism is CH + CHO→CHCHO→C_2H_2 + O + (H)→CH_2CH + O + (H)→CH_3CH + O + (H)→ CH_3CH_2 + O + (H)→$\mathbf{C_2H_6}$ + O. However, it is noted that the optimal route of C_2H_6 formation *via* CHO insertion mechanism is kinetically unfavorable than C_2H_6 formation *via* the carbide mechanism with the route of CH self-coupling (171.5 ***vs.*** 111.8 kJ·mol^{-1}).

The results mentioned above indicated that C_2H_6 formation mainly goes through the carbide mechanism with CH self-coupling instead of CHO insertion mechanism on the Co(10–12) facet, which agrees with that on the Co(10-10) [13] and (10–11) facets [14] that the carbide mechanism *via* CH or CH_2 self-coupling primarily contributes to C_2H_6 formation. In contrast, the formation of C_2H_6 on the Co(111) [18] and (0001) facets [35] mainly goes through CHO insertion mechanism.

3.2.2.3. The effect of methane and ethanol formation on C_2 hydrocarbons. As depicted in Fig. 5, beginning with the CH monomer, methane is produced by CH successive hydrogenation requiring an overall energy barrier of 121.2 kJ·mol^{-1} (red line), which is slightly higher than C_2 hydrocarbons CH_3CH, CH_3CH_2 and C_2H_6 (98.9, 103.0 and 111.8 kJ mol^{-1}). As shown in Fig. 6, the preferred route of ethanol formation (green line) is CH + CO + H→CH + CHO→CHCHO + (H)→CH_2CHO + (H)→ CH_3CHO + (H)→CH_3CH_2O + (H)→ethanol with much higher overall energy barrier (221.5 kJ·mol^{-1}) than CH_3CH, CH_3CH_2 and C_2H_6 formation on Co(10–12) facet.

Thus, methane formation reduces the production of C_2 hydrocarbons on Co(10–12) facet, and identical conclusions were also obtained in the previous studies that methane has an obvious effect on the formation of C_2 hydrocarbons on Co(10–11) [14] and (111) facets [18]. However, ethanol formation by CHO insertion mechanism is much unfavorable in kinetics, namely, ethanol has a negligible effect on the selectivity of C_2 hydrocarbons over Co(10–12) facet, which also agree with the observation over the Co(10–11) [14] and (111) facets [18].

3.2.2.4. The formation of C_3 species from C_2 species. As mentioned above, for the formation of C_2 species from C_1 species, the CH_x (x = 0 ~ 3)-related reactions including the coupling, CHO/CO insertion and hydrogenation have been examined on the Co(10–12) facet, the results show that CHO insertion into CH_x is more favored in kinetics compared to CO insertion into CH_x, which is also supported by the results from the previous studies, for example, the theoretical researches by Zhao et al. [12] and Wen et al. [35] clarified that the carbon chain formation on the Co(0001) facet is mainly attribute to CHO insertion into CH_x rather than CO insertion into CH_x; Chen et al. [18] believed that CHO insertion mechanism was more reasonable for the carbon chain formation on the flatted Co(111) facet, moreover, CHO formation was facilitated on the stepped Co(111) facet. Namely, CHO insertion mechanism is more favored in kinetics compared to CO insertion mechanism. On the other hand, Weststrate et al. [52] recently

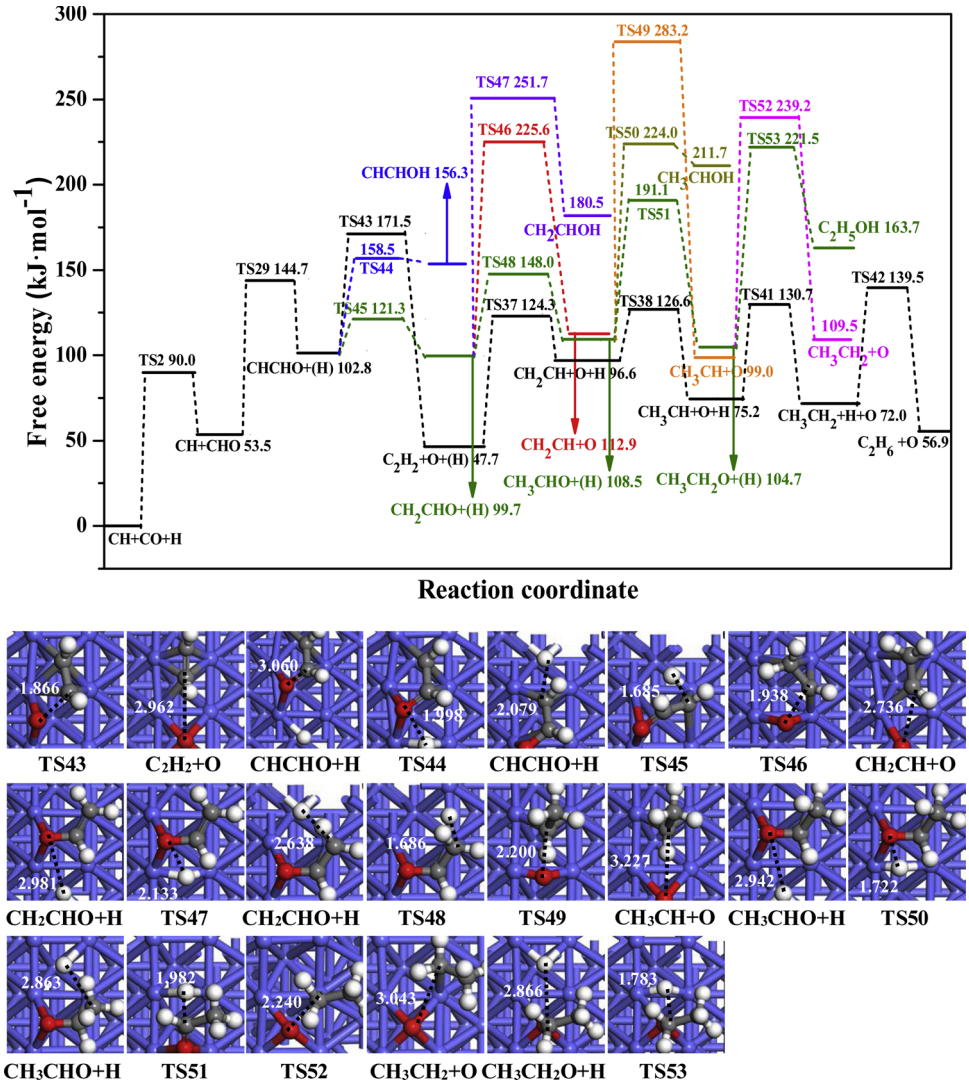

Fig. 6. The free energy profile of the reactions related to CH_xCHO with respect to the CH + CO + H species at 500 K together with the structures of initial states (ISs), transition states (TSs) and final states (FSs) on the Co(10-12) facet. Bond lengths are in Å.

identified the C—C bond formation mechanism on Co catalyst using in-situ high resolution X-ray photoelectron spectroscopy; the results show that CO promotes the chain growth by stabilizing the intermediates instead of participating in the C—C bond formation, and the carbon chain growth in experiment follows the carbide mechanism. Moreover, the DFT studies by Cheng et al. [10,11] over the stepped Co(0001) facet showed that the favorable carbon chain growth pathway of $C_2 \rightarrow C_3$ and $C_3 \rightarrow C_4$ species are similar to that of $C_1 \rightarrow C_2$ species, that is, $RCH_2 + C$ and $RCH_2CH + CH_2$ are the most possible $C_2 + C_1$ and $C_3 + C_1$ coupling reactions, $CH_3 + C$ and $CH_2 + CH_2$ are the major chain growth pathways of $C_1 + C_1$ coupling. Further, in our previous studies about carbon chain growth mechanism over the Co(10-10) [13], (10–11) [14] and (0001) [35] facets, for the formation of C_2 hydrocarbons, CHO insertion into CH_x is more favored in kinetics compared to CO insertion into CH_x, moreover, for the formation of C_3 species from C_2 species, the carbide mechanism is the major pathway over the Co(10-10) and (10–11) facets; meanwhile, CHO insertion mechanism with CHO insertion into CH/CH_2, CH_3CH and CH_3CH_2CH to form $CHCHO/CH_2CHO$, CH_3CHCHO and CH_3CH_2CHCHO are more preferred to realize the carbon chain growth on the Co(0001) facet.

As depicted in Fig. 5, the optimal formation route of CH_3CH is $CH + CH + (H) \rightarrow C_2H_2 + (H) \rightarrow CH_2CH + (H) \rightarrow \mathbf{CH_3CH}$ requiring an overall energy barrier of 98.9 kJ·mol^{-1}; CH_3CH_2 is $CH + CH \rightarrow C_2H_2 + (H) \rightarrow CH_2CH + (H) \rightarrow CH_3CH + (H) \rightarrow \mathbf{CH_3CH_2}$ requiring an overall energy barrier of 103.0 kJ·mol^{-1}. Namely, both CH_3CH and CH_3CH_2 are abundant C_2 intermediates in the process of C_2H_6 formation over the Co(10–12) facet. Therefore, beginning with the CH_3CH and CH_3CH_2 intermediates, the formation of C_3H_8 and propanol *via* the carbide mechanism and CHO insertion mechanism are examined over the Co(10–12) facet (see details in the Supplementary Material).

3.2.2.5. C_3H_8 formation via the carbide mechanism. CH_3CH and CH_3CH_2 acted as the major C_2 intermediates possibly couple with the stable CH_x species to achieve the growth of carbon chain from the C_2 to C_3 species. As illustrated in Fig. 7, beginning with the $CH_3CH + CH + H$ species, CH_3CH is preferentially hydrogenated to produce CH_3CH_2 instead of its coupling with CH to CH_3CH_2CH (55.5 ***vs.*** 163.7 kJ·mol^{-1}), subsequently, CH_3CH_2 could react with CH (red line) or CH_2 (black line) to produce CH_3CH_2CH or $CH_3CH_2CH_2$, followed by their hydrogenations to produce C_3H_8, which correspond to the overall energy barriers of 114.9 or 58.2 kJ·mol^{-1}, respectively, suggesting that C_3H_8 is preferentially produced *via* the route $CH_3CH + H + CH_2 \rightarrow CH_3CH_2 + CH_2 + (H) \rightarrow CH_3CH_2CH_2 + (H) \rightarrow C_3H_8$ requiring an overall energy barrier of 58.2 kJ·mol^{-1}. Accordingly, starting with CH_3CH_2 intermediate, C_3H_8 formed by $CH_3CH_2 + CH_2 + H \rightarrow CH_3CH_2CH_2 + H \rightarrow C_3H_8$ is dynamically competitive

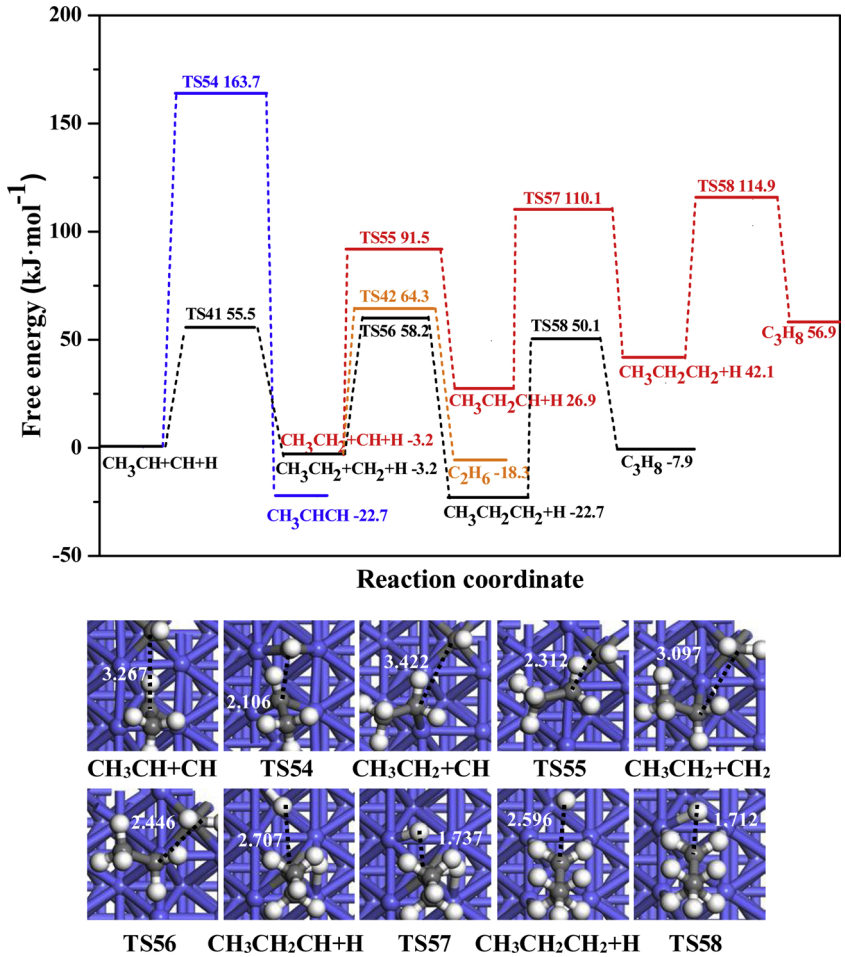

Fig. 7. The free energy profile of C_3H_8 formation *via* the carbide mechanism together with the structures of initial states (ISs), transition states (TSs) and final states (FSs) on the Co(10-12) facet. Bond lengths are in Å.

with C_2H_6 formation *via* CH_3CH_2 hydrogenation (61.4 ***vs.*** 67.5 kJ·mol^{-1}), thus, the coupling of CH_3CH_2 and CH_2 can achieve the carbon chain growth during the formation of C_3H_8.

3.2.2.6. C_3H_8 formation via the CHO insertion mechanism. Starting from the CH_3CH and CH_3CH_2 intermediates, CHO inserts into CH_3CH and CH_3CH_2 to form CH_3CHCHO and CH_3CH_2CHO, respectively. See Fig. 8a, CH_3CHCHO hydrogenation to CH_3CH_2CHO is superior to its hydrogenation to $CH_3CHCHOH$ and its dissociation into CH_3CHCH (80.0 ***vs.*** 143.2 and 107.4 kJ·mol^{-1}), then, CH_3CH_2CHO dissociation into CH_3CH_2CH is much easier in kinetics than its hydrogenation to CH_3CH_2CHOH and $CH_3CH_2CH_2O$ (79.8 ***vs.*** 144.9 and 118.5 kJ·mol^{-1}). Further, as presented in Fig. 8b, starting from CH_3CH + CO + H species, the overall energy barriers of C_3H_8 formation by $CH_3CH_2CH_2$ hydrogenation *via* the CH_3CHCHO (red line) and CH_3CH_2CHO (black line) intermediates are close (138.0 ***vs.*** 143.8 kJ·mol^{-1}) in the CHO insertion mechanism, which are much higher than that *via* the carbide mechanism (58.2 kJ·mol^{-1}).

Thus, C_3H_8 formation *via* the carbide mechanism is more favored in kinetics than the CHO insertion mechanism (58.2 ***vs.*** 143.8/138.0 kJ·mol^{-1}) on Co(10–12) facet, in which $CH_3CH_2CH_2$ intermediate is the most abundance C_3H_x species produced by the carbide mechanism requiring an overall energy barrier of 58.2 kJ·mol^{-1}. Further, the carbide mechanism dominantly contribute to C_3 hydrocarbons formation on the Co(10-10) [13] and (10–11) facets [14]; while the CHO insertion mechanism is mainly responsible for C_3 hydrocarbons formation on Co(0001) facet [35].

3.2.2.7. The effect of propanol formation on C_3 hydrocarbons. As shown in Fig. 8b, propanol produced by the route of CH_3CH + CHO + (H)→ CH_3CHCHO + (H) or CH_3CH_2 + CHO + (H)→CH_3CH_2CHO + (H)→ $CH_3CH_2CH_2O$ + (H) →propanol is much unfavorable in kinetics than C_3H_8 formation (175.9 and 208.1 ***vs.*** 58.2 kJ·mol^{-1}). Thus, propanol formation can be significantly inhibited in the process of C_3H_x formation ($CH_3CH_2CH_2$ and C_3H_8) on Co(10–12) facet. In addition, previous studies also verified that propanol has a negligible effect on the formation of C_3 hydrocarbons over the Co(10-10), (10–11) and (0001) facets [13,14,35].

3.2.3. The formation of C_4 species from C_3 species on the Co(10–12) facet

Since $CH_3CH_2CH_2$ species is the favored C_3H_x intermediate on Co (10–12) facet, to gain a better understanding about carbon chain formation of C_4 species from C_3 species, starting from $CH_3CH_2CH_2$ intermediate, the hydrogenation, CHO insertion and CH_2 coupling were calculated (see Fig. 9). $CH_3CH_2CH_2$ coupling with CH_2 to $CH_3CH_2CH_2CH_2$ is more preferred in kinetics than CHO insertion into $CH_3CH_2CH_2$ and $CH_3CH_2CH_2$ hydrogenation (24.9 ***vs.*** 80.5 and 72.8 kJ·mol^{-1}). Moreover, C_4H_{10} formation by $CH_3CH_2CH_2CH_2$ hydrogenation is much easier in kinetics than CHO insertion into $CH_3CH_2CH_2$ and $CH_3CH_2CH_2$ hydrogenation (34.6 ***vs.*** 80.5 and 72.8 kJ·mol^{-1}), thus, C_4H_{10} formation dominantly goes through the carbide mechanism on Co(10–12) facet.

For the butanol formation, the overall energy barrier of $CH_3CH_2CH_2CHO$ formation, a key intermediate in butanol formation, is much higher than that of C_4H_{10} formation (80.5 ***vs.*** 34.6 kJ·mol^{-1}), thus, butanol formation is unfavorable on the Co(10–12) facet, which

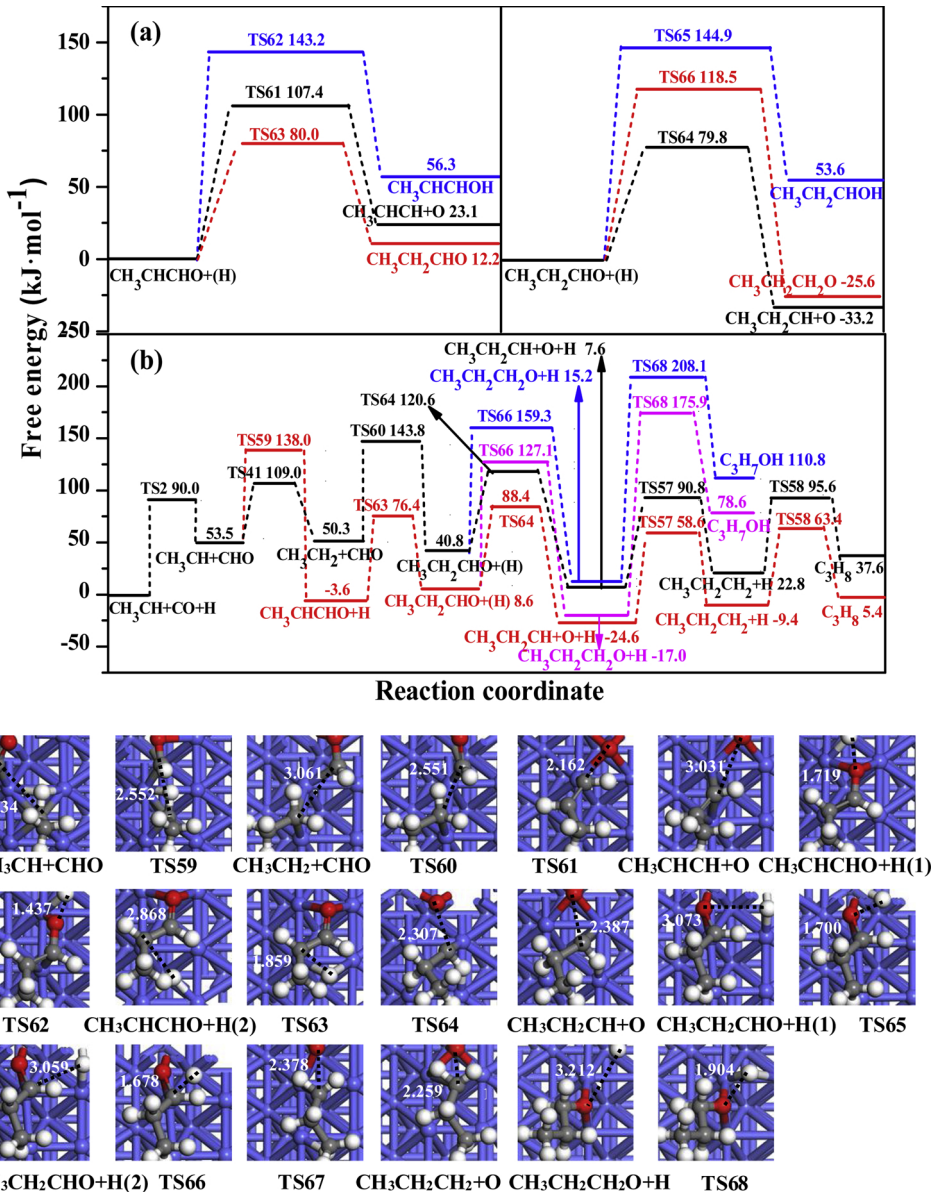

Fig. 8. The free energy profile of C_3H_8 and C_3H_7OH formation *via* the CHO insertion mechanism together with the structures of initial states (ISs), transition states (TSs) and final states (FSs) on the Co(10-12) facet. Bond lengths are in Å.

has a negligible effect on C_4H_x formation ($CH_3CH_2CH_2CH_2$ and C_4H_{10}).

3.2.4. Microkinetic modeling on the Co(10–12) facet

Aiming at further quantitatively obtain the influence of methane and alcohols on the C_{2+} hydrocarbons under the realistic conditions, the microkinetic modeling [53–55] is employed to qualitatively understand the selectivity of major products (CH_3OH, CH_4, C_2H_5OH, C_2H_4, C_2H_6, C_3H_7OH, C_3H_8 and C_4H_{10}) under the experimental conditions of FTS reactions (P_{CO} = 5 atm, P_{H_2} = 10 atm and T = 500 K) (see details in the Supplementary Material). Moreover, for the kinetics of surface reactions, we only considered the forward reaction, which is a safe approximation at such high pressures of CO and H_2 as we use experimentally [54–56]. In addition, it is noted that aiming at considering the effects of reaction temperature and pressure on reaction activity and selectivity of FTS reaction, although a larger number of previous studies [54–61] have shown that the applications of microkinetic models combined with energy data obtained by DFT calculations have achieved significant progress for the FTS reaction, the simple microkinetic model assumes that there are no interactions between adsorbate-adsorbate using the mean-field theory. In fact, for the high-coverage system, the coverage effect becomes highly complex and cannot be ignored, for example, the previous studies about the coverage-dependent kinetic model adopted by Lausche et al. [62] and Hu et al. [63] have shown that the adsorbate-adsorbate interactions have a greatly influence on the coverage of reaction intermediates, then affect activity and products selectivity in the FTS reaction. However, this study mainly focus on the comparisons about the carbon chain growth mechanism of FTS reactions among the mostly exposed hcp Co(10–12) and our previous (10-10) [13], (10–11) [14], (0001) [35] and fcc Co(111) [18] facets, since our previous studies do not examine the effects of adsorbate-adsorbate interactions, the effects of adsorbate-adsorbate interactions on the coverage of reaction intermediates, as well as the activity and products selectivity in the FTS reaction are also not considered over the Co (10–12) facet, which will be considered in our future work.

The relative selectivity of CH_4, C_2H_4, C_2H_6, C_3H_8 and C_4H_{10} are 25.20 %, 0%, 0%, 0% and 74.79 %, respectively, that of CH_3OH, C_2H_5OH and C_3H_7OH are negligible, suggesting that alcohols have a negligible effect on C_{2+} hydrocarbons. Meanwhile, compared to C_2H_4,

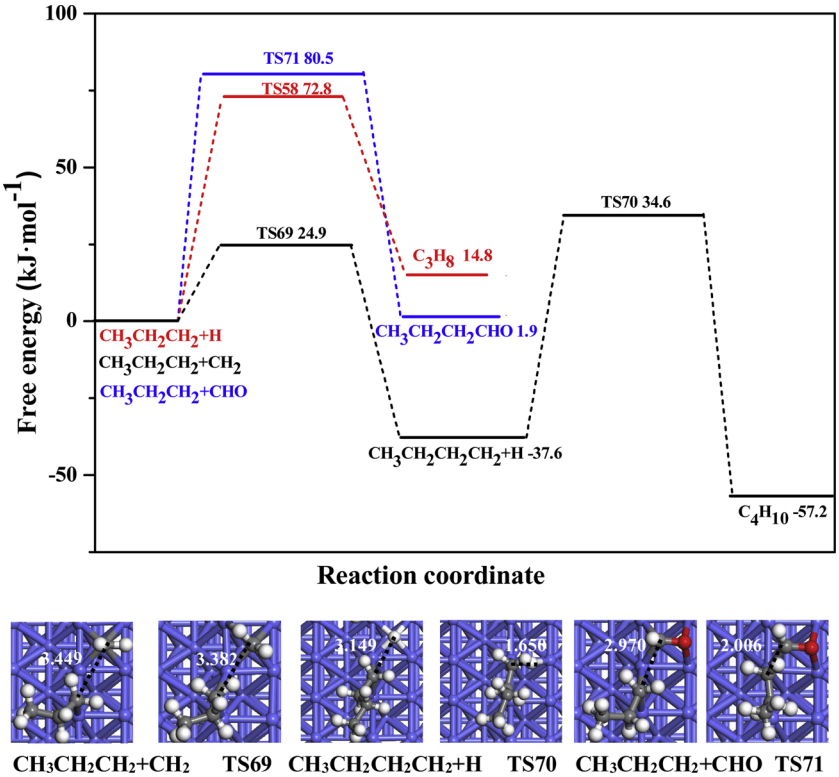

Fig. 9. The free energy profile for the formation of C_4 hydrocarbons together with the structures of initial states (ISs), transition states (TSs) and final states (FSs) on the Co(10-12) facet in FTS. Bond lengths are in Å.

C_2H_6 and C_3H_8, the much higher C_4H_{10} selectivity means that the Co (10–12) facet is extremely beneficial for the formation of longer carbon chain, which is in accordance with the previous experimental observations [64,65]. Thus, the Co(10–12) facet goes through carbide mechanism to exhibit highly catalytic activity and selectivity for C_{2+} hydrocarbons; moreover, an effective strategy to promote carbon chain growth on Co(10–12) facet should be focused on inhibiting methane formation in the FTS reactions.

Further, an in-depth analysis for the effects of the coverage of the surface species in the microkinetic modeling are carried out, and the coverages of key intermediates involving in the carbon chain growth from the C_1 to C_4 species on the Co(10–12) facet are presented in Table S5. It can be obtained from DFT calculation that the selectivity-determined step for C_4 hydrocarbon formation is CH hydrogenation, CH coupling and CHO insertion into CH. By comparing the coverage of key intermediates (CH, H and CHO) involved in the selectivity-determined step for C_4 hydrocarbon formation, it can be obtained that the coverage of CH species is much higher by 4 and 8 orders of magnitude than that of CHO and H species, as a result, CH self-coupling to form C_2H_2 preferentially occurred and promote carbon chain growth. Similarly, in the formation process of C_3 and C_4 chain, considering the coverage of key intermediates (CH_3CH/CH_3CH_2, $CH_3CH_2CH_2$, CH_2 ***vs.*** CHO, H) and reaction rate constants (k_{56}/k_{69} ***vs.*** k_{60}/k_{71} and k_{42}/k_{58}), the C_2 and C_3 intermediates (CH_3CH/CH_3CH_2 and $CH_3CH_2CH_2$) preferentially couple with CH_2 and promote the growth of carbon chain to produce C_4 hydrocarbons. Therefore, the rate constants of elementary reactions and the relative coverage of key intermediates in the selectivity-determined step are two key factors to determine the selectivity of products in the FTS reactions.

3.3. The carbon chain growth mechanism over different Co facets

The optimal formation route of C_4 hydrocarbons from syngas on Co (10–12) facet is summarized in Fig. 10. Both CH and CH_2 as the dominant CH_x monomers are more inclined to undergo their self-coupling (carbide mechanism) to realize the initial carbon chain formation; meanwhile, both CH_3CH and CH_3CH_2 intermediates as the stable C_2H_x species can continuously contribute to carbon chain growth from the C_2 to C_3 and C_3 to C_4 species *via* the carbide mechanism that CH_3CH_2 coupling with CH_2 to $CH_3CH_2CH_2$ and $CH_3CH_2CH_2$ coupling with CH_2 to $CH_3CH_2CH_2CH_2$. Therefore, it is concluded that RCH_2(R=H/alkyl) acted as the abundant intermediate could couple with CH_2 *via* the carbide mechanism to form $R'CH_2$(R'=RCH_2) over Co(10–12) facet, which realize the carbon chain growth; further, the carbon chain growth is terminated once the hydrogenation of $R'CH_2$ into alkane is more favorable than $R'CH_2$ coupling with CH_2. In addition, methane and alcohols can be formed by CH_x hydrogenation and CHO insertion mechanism in the process of carbon chain growth, the effect of alcohols on the C_{2+} hydrocarbons is negligible, while methane formation affects the selectivity and productivity of C_{2+} hydrocarbons.

Our previous studies showed that the formation of C_{2+} hydrocarbons on the Co(10–11) [14] and (10-10) facets [13] were accomplished by the carbide mechanism that the coupling of RCH_2(R=H/alkyl) and CH_2 can produce $R'CH_2$(R'=RCH_2). However, the carbon chain growth over the Co(0001) [12,35], as well as the flat and stepped Co(111) facets [18] was dominantly realized by the CHO insertion mechanism with the cycle of RCH(R=H/alkyl) inserted by CHO to form RCHCHO and its C—O bond breakage.

3.4. The effect of Co crystal structures on the catalytic performance

3.4.1. The effect of Co crystal structures on the carbon chain growth mechanism

Beginning with CO+H species, C_{2+} hydrocarbons are formed by two key steps, one is CO activation to produce CH_x, the other is the initial formation and growth of carbon chain. To gain more insight into the influence of Co crystal structures on the carbon chain growth mechanism, the results over the hcp Co(10–12) facet in this work are compared with our previous results on the hcp Co(0001) [35], (10-10) [13], (10–11) [14] and fcc Co(111) facets [18].

For CO activation to produce CH_x(x = 1 ~ 3), on the hcp Co(10–12) and (10–11) [14] facets, the favored CH monomer is produced by CO

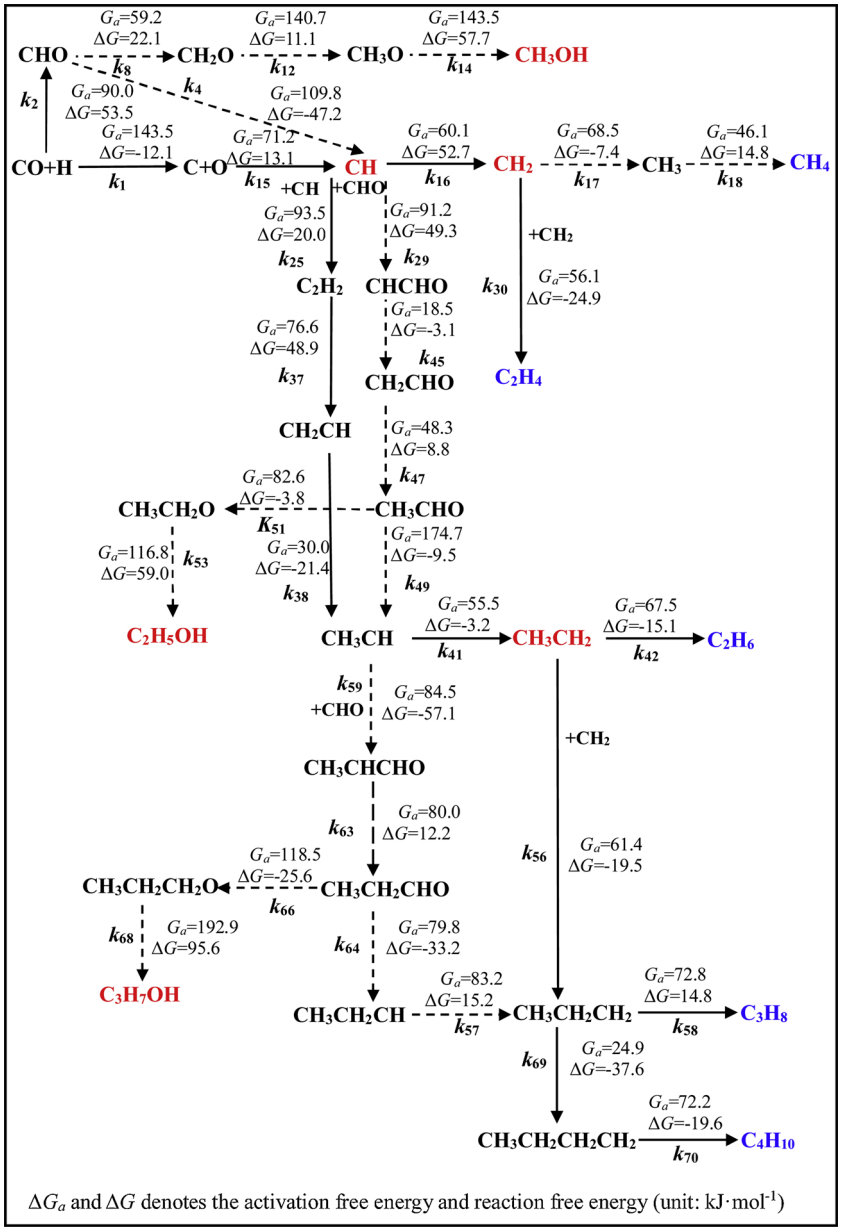

Fig. 10. The optimal formation pathway of the hydrocarbons from the C_1 to C_4 species from syngas involved in the FTS reactions on the Co(10-12) facet. The dash line corresponds to the optimal formation pathway of $C_2 \sim C_4$ hydrocarbons; the solid lines refer to the optimal formation pathway of methane and $C_1 \sim C_3$ alcohols.

direct dissociation and hydrogenation requiring the overall energy barriers of 143.5 and 153.7 kJ·mol^{-1}, respectively. In contrast, on the hcp Co(10-10) facet [13], CH_2 as the dominant monomer is preferentially produced by CO hydrogen-assisted dissociation *via* the CH_2O intermediate, which requires an overall energy barrier of 132.3 kJ·mol^{-1}. On the hcp Co(0001) facet [35], both CH and CH_2 produced by CO hydrogen-assisted dissociation *via* the CHO intermediate are the dominant monomers, which requires an overall energy barrier of 189.4 kJ·mol^{-1}, and CH_2 is formed by CH hydrogenation. On the fcc Co(111) facet [18], the dominant CH_x monomers are CH and CH_2, which are mainly produced by CO hydrogen-assisted dissociation *via* the CHO and CH_2O intermediates, respectively; the formation of CH and CH_2 have the overall energy barriers of 177.0 and 193.1 kJ·mol^{-1}, respectively. On the other hand, Liu et al. [29] found that CO activation to form CH monomer goes through CO hydrogen-assisted dissociation *via* the CHO intermediates on the most active fcc Co(110), (100) and (311) facets, whereas the hcp Co(11–21), (10–11), (10–12) and (11–20) facets prefer to be CO direct dissociation; meanwhile, the hcp Co (11–21), (10–11), (10–12) and (11–20) facets present the higher intrinsic activity for CO activation to form CH monomer than the fcc Co (110), (100) and (311) facets; moreover, Lyu et al. [66] have obtained the contribution of different facets to CO activation in Wulff construction and estimated that the hcp Co presents lower activation energy than the fcc Co (1.14 ***vs.*** 1.48 eV). In addition, CO activation on the fcc (321) and (221) facets with the kink and step sites was further studied by Petersen et al. [67], and the comparison of the relative rates of direct CO dissociation on fcc Co facets (Co(321), (211), (311), (221), (111), (100)) confirms that the step and kink defect sites are more active for CO activation. However, the increase in the activity of fcc Co with the step and kink defect sites (Co(321), (211), (311) and (221) facets) is still lower than that of highly active hcp Co(10–11) and (11–21) facets. Therefore, either the formation mechanism of $CH_x(x = 1 \sim 3)$ species or the dominant existence form of CH_x monomer are affected by the crystal structure of Co catalysts; more importantly, according to the surface area proportion of the various facets exposed on hcp and fcc Co from Wulff construction, it is concluded that the Co(10-10), (10–11),

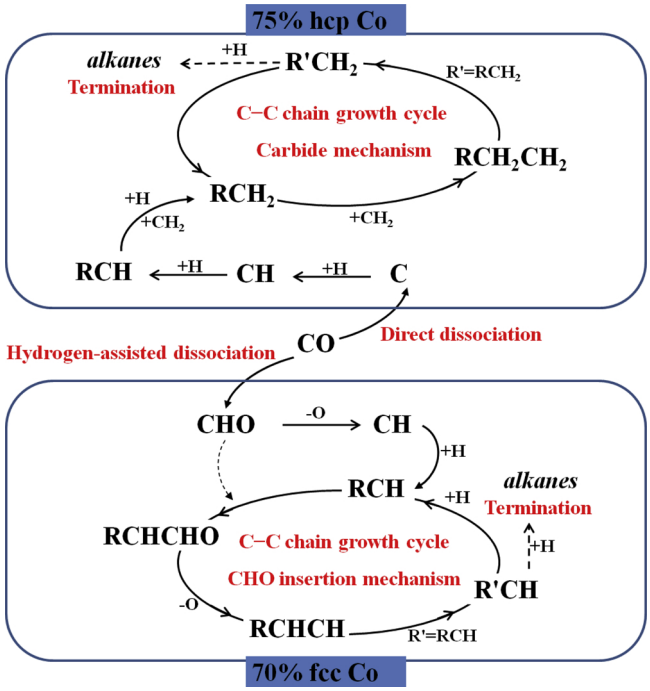

Fig. 11. The proposed mechanism for the initiation, growth and termination of the C−C chain from syngas on the hcp and fcc Co catalysts. R represents hydrogen or an alkyl group.

(10–12) and (11–20) facets occupied 28 %, 35 %, 12 % and 6% total exposed areas of hcp Co crystal phase present higher catalytic activity toward $CH_x(x = 1 \sim 3)$ formation compared to the Co(111), (100), (311) and (110) facets occupied 70 %, 12 %, 10 % and 8% total exposed areas of fcc Co crystal phase.

For the initial formation and growth of carbon chain over the Co catalysts, the preferred mechanism depends on the Co crystal structures. As summarized in Fig. 11, on the 75 % hcp Co facets (28 % (10-10) [13], 35 % (10–11) [14] and 12 % (10–12)), the carbide mechanism mainly leads to the carbon chain growth to produce higher carbon hydrocarbons $R'CH_2(R' = RCH_2)$ *via* the coupling of RCH_2 with CH_2. However, on the 18 % hcp Co(0001) [35] and 70 % fcc Co(111) [18] facets, the CHO insertion mechanism mainly facilitate carbon chain growth through the cycle that CHO insertion into RCH to RCHCHO, followed by the C−O bond cleavage of RCHCHO to R'CH(R' = RCH). In addition, the previous DFT studies by Li et al. [50] also showed that the carbon chain growth followed CO insertion mechanism without considering CHO insertion mechanism on Co(0001) facet, and the carbide mechanism is preferable on Co(10–11) facet accompanied with higher selectivity of C_2 hydrocarbons than CH_4.

Therefore, according to the occupied proportion of these crystal structures in Co crystal phases [29], the relationship between Co crystal structure and the mechanism of C_{2+} hydrocarbons formation can be obtained, CO direct dissociation and carbide mechanism dominantly contribute to the production of C_{2+} hydrocarbons over the hcp Co catalysts; while CO hydrogen-assisted dissociation and CHO insertion mechanism is mainly responsible for the formation of C_{2+} hydrocarbons over the fcc Co catalysts. Moreover, CHO formed by CO hydrogenation is thermodynamically unstable, which may limited the interactions between CHO and CH_x intermediates due to a relatively low CHO coverage [29,68], as a result, the carbon chain growth is unfavorable over the 18 % hcp Co(0001) [35] and 70 % fcc Co(111) facets [18] compared to the 75 % hcp Co facets. Accordingly, compared to the fcc Co catalyst, the hcp Co catalyst exhibits higher catalytic activity for C_{2+} hydrocarbons formation, which is supported by the previous studies that the hcp Co catalysts were more favorable for CO activation and conversion than the fcc Co catalysts [28–30,69–71].

3.4.2. The effects of methane and alcohols over the hcp and fcc Co

Given that the formation of CH_x species and the growth of carbon chain are accompanied by the formation of methane and alcohols in the FTS reactions, which may reduce the selectivity of C_{2+} hydrocarbons. The results about the effects of methane and alcohols on C_{2+} hydrocarbons formation over the hcp Co(10–12) facet in this work are compared with our previous results on the hcp Co(10-10) [13], (10–11) [14], (0001) [35] and fcc Co(111) [18] facets.

For the effect of methane, the relative selectivity of methane is 17.72 %, 25.53 % and 25.20 % on the hcp Co(10-10) [13], (10–11) [14] and (10–12) facets, which is much lower than that of C_{2+} hydrocarbons; however, the relative selectivity of methane is higher on the hcp Co(0001) facet [35] compared to the other hcp Co facets. Moreover, methane formation is extremely active than C_2 hydrocarbons over the fcc Co(111) facet [18]. In general, methane affects the selectivity and productivity of C_{2+} hydrocarbons in the FTS reactions over the Co catalysts, and its effect on the fcc Co catalysts is more obvious than that on the hcp Co catalysts.

For the effect of alcohols, the hcp Co(0001) [35], (10-10) [13], (10–11) [14] and (10–12) facets present higher activity and selectivity for $CH_x(x = 1 \sim 3)$ formation instead of methanol; then, the formation of total alcohols has a negligible influence on the selectivity and productivity of C_{2+} hydrocarbons over the hcp Co(0001) [35], (10-10) [13], (10–11) [14] and (10–12) facets. That is, the influence of alcohols on the C_{2+} hydrocarbons formation over the hcp Co catalysts is negligible. However, on the fcc Co(111) facet [18], although CH_x $(x = 1 \sim 3)$ formation is more favored than methanol, the production of ethanol reduces the selectivity of C_2 hydrocarbons. Therefore, the influence of alcohols species on the selectivity and productivity of C_{2+} hydrocarbons over the fcc Co catalyst is more obvious than that over the hcp Co catalysts, which is supported by the experimental observation from Gnanamani et al. [72] that the hcp Co catalysts not only exhibit higher activity for FTS reactions, but also produce less methane and more C_{5+} hydrocarbons compared to the fcc Co catalysts. Moreover, the recent experiment studies [48] also confirmed that the Co (10–11) facet exhibits the highest catalytic activity and selectivity for the formation of C_{5+} hydrocarbons and the lowest methane selectivity in the FTS reactions.

3.4.3. Structure-performance relationship of Co catalyst for carbon chain growth

In order to further reveal the microscopic reasons that the crystal structures affect the carbon chain growth mechanism, the active unit (defined as the smallest structural unit consisted of the active site) to reflect structure characteristics of different crystal facets was proposed (see Fig. 12): the crystal facet structures containing the stepped B_5-type active unit consisted of five Co atoms (such as Co(10-10), (10–11) and (10–12) facets) could promote carbon chain growth *via* the carbide mechanism, whereas the crystal facet structures containing the flatted 4-fold active unit consisted of four Co atoms (such as (111) and (0001) facets) contribute to carbon chain growth *via* the CHO insertion mechanism. Hence, it is proposed that regulating the crystal facet structure of Co catalysts can well control the catalytic performance of carbon chain growth in the FTS reactions, especially, when the hcp Co(10-10), (10–11) and (10–12) facets with more stepped B_5-type active unit can be acquired, it will facilitate the formation of long-chain hydrocarbons. Recently, the experimental studies [48] further confirmed our proposed predications that the Co(10–11) facet exhibits the highest catalytic activity and selectivity for the formation of C_{5+} hydrocarbons in the FTS reactions and the lowest methane selectivity.

Overall, according to the occupied proportion of different crystal facets in the hcp and fcc Co crystal phases, the hcp Co presents much higher intrinsic activity for CO activation to produce key CH_x intermediate *via* CO direct dissociation mechanism and carbon chain growth

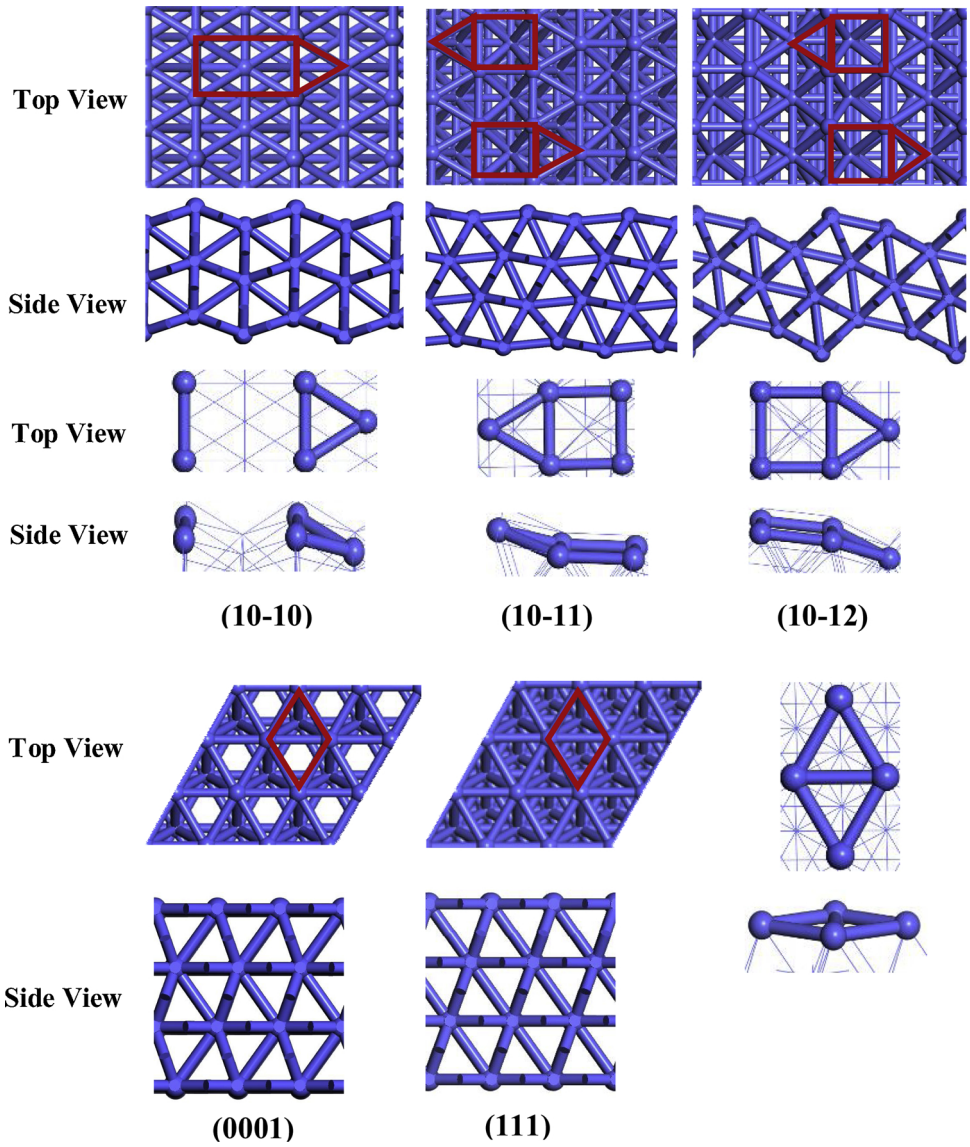

Fig. 12. The active unit structure for different crystal facets of hcp and fcc Co catalysts.

via the carbide mechanism; whereas the fcc Co present lower intrinsic activity *via* hydrogen-assisted CO dissociation and CHO insertion mechanism. Thus, the hcp Co should be the preferable phase for the rational design of Co catalyst. Interestingly, the recent experiment studies [66] also verified our calculated conclusions that the hcp Co exhibits high activity toward C_{5+} hydrocarbons formation than the fcc Co, the Co(10–11) facet exhibits the highest catalytic activity and selectivity for the formation of C_{5+} hydrocarbons in the FTS reactions and the lowest methane selectivity, in which the single-phase Co catalysts with high purity were for the first time synthesized and experimentally verified. This work also reminds us that more attention should be paid to the real state of Co crystal facet structures in the catalysis process of FTS reactions.

4. Conclusions

In this study, aiming at identifying the relationship between Co crystal facet structure and the catalytic performance of carbon chain growth in the FTS reactions, the preferential mechanism involving in carbon chain growth from C_1 to C_4 species over the hcp and fcc Co catalysts is systematically studied by DFT calculations, meanwhile, the exposed (0001), (10-10), (10–11) and (10–12) facets occupying 93 % of total surface area for the hcp Co, as well as the dominantly exposed (111) facet occupying 70 % of total surface area for the fcc Co are considered. The results show that for CO activation to form CH_x monomer as the key intermediate in the carbon chain growth, the crystal phase and facet of Co catalysts affect the preferred formation route of favored $CH_x(x = 1 \sim 3)$ monomer and therefore alter its dominant existence form, the hcp Co catalyst presents much higher intrinsic activity than the fcc Co catalyst. During the process of carbon chain growth, the effects of methane and alcohols on the formation of C_{2+} hydrocarbons are sensitive to Co crystal phase and facet, methane formation has a certain influence on the selectivity and productivity of C_{2+} hydrocarbons in the FTS reaction over Co catalysts irrespective of the hcp and fcc crystal pahse; however, the influence of alcohols over the hcp Co catalyst is negligible, whereas that should be considered over the fcc Co catalyst. Generally, for the carbon chain growth, the effects of methane and alcohols over the hcp Co catalyst are much lower than that over the fcc Co catalyst.

According to the occupied proportion of these crystal facets in the hcp or fcc Co crystal phase, the dependence of carbon chain growth mechanism on Co crystal structure are obtained, that is, the hcp Co(10-10), (10–11) and (10–12) facets with the stepped B_5-type active unit dominantly goes through the carbide mechanism to promote carbon

chain growth, whereas the fcc Co(111) and hcp Co(0001) facets with the flatted 4-fold active unit mainly undergoes the CHO insertion mechanism to promote carbon chain growth. However, CHO formation is thermodynamically unstable resulting in the relatively low coverage, which limits the interactions between CHO and C_nH_x intermediate. As a result, the carbon chain growth is unfavorable on the hcp Co(0001) and fcc Co(111) facets compared to that over other hcp Co facets. Thus, synthesizing Co crystal facet with more stepped B_5-type active unit in the FTS reaction would be highly valuable due to the higher mass-specific reactivity, such as, the hcp Co(10-10), (10–11) and (10–12) facets.

CRediT authorship contribution statement

Riguang Zhang: Conceptualization, Investigation, Visualization, Formal analysis, Writing - original draft, Writing - review & editing. **Li Kang:** Investigation, Writing - review & editing. **Hongxia Liu:** Writing - original draft, Formal analysis. **Baojun Wang:** Project administration, Resources, Supervision, Funding acquisition. **Debao Li:** Formal analysis, Investigation. **Maohong Fan:** Project administration, Resources, Supervision, Funding acquisition.

Declaration of Competing Interest

The authors declare that they have no known competing financial interests or personal relationships that could have appeared to influence the work reported in this paper.

Acknowledgments

This work is financially supported by the Key Projects of National Natural Science Foundation of China (21736007), National Natural Science Foundation of China (21776193 and 21476155), the China Scholarship Council, and the Top Young Innovative Talents of Shanxi. Also, authors appreciate the support of University of Wyoming.

Appendix A. Supplementary data

Supplementary material related to this article can be found, in the online version, at doi:https://doi.org/10.1016/j.apcatb.2020.118847.

References

[1] P. Biloen, W.M.H. Sachtler, Mechanism of hydrocarbon synthesis over Fischer-Tropsch catalysts, J. Adv. Catal. Sci. Technol. 30 (1981) 165–216.
[2] H. Jahangiri, J. Bennett, P. Mahjoubi, K. Wilson, S. Gu, A review of advanced catalyst development for Fischer-Tropsch synthesis of hydrocarbons from biomass derived syngas, Catal. Sci. Technol. 4 (2014) 2210–2229.
[3] E. Van Steen, M. Claeys, Fischer-Tropsch catalysts for the biomass-to-liquid process, Chem. Eng. Technol. 31 (2008) 655–666.
[4] F. Fischer, H. Tropsch, The synthesis of petroleum at atmospheric pressures from gasification products of coal, Brennst. Chem. 7 (1926) 97–104.
[5] J. Yang, E.Z. Tveten, D. Chen, A. Holmen, Understanding the effect of cobalt particle size on Fischer-Tropsch synthesis: surface species and mechanistic studies by ssitka and kinetic isotope effect, Langmuir 26 (2010) 16558–16567.
[6] J.P. Den Breejen, P.B. Radstake, G.L. Bezemer, J.H. Bitter, V. Frøseth, A. Holmen, K.P. De Jong, On the origin of the cobalt particle size effects in Fischer-Tropsch catalysis, J. Am. Chem. Soc. 131 (2009) 7197–7203.
[7] G.L. Bezemer, J.H. Bitter, H.P.C.E. Kuipers, H. Oosterbeek, J.E. Holewijn, X.D. Xu, F. Kapteijn, A.J. van Dillen, K.P. De Jong, Cobalt particle size effects in the Fischer-Tropsch reaction studied with carbon nanofiber supported catalysts, J. Am. Chem. Soc. 128 (2006) 3956–3964.
[8] P. Biloen, J.N. Helle, W.M.H. Sachtler, Incorporation of surface carbon into hydrocarbons during Fischer-Tropsch synthesis: mechanistic implications, J. Catal. 58 (1979) 95–107.
[9] R.A. Van Santen, A.J. Markvoort, Chain growth by CO insertion in the Fischer-Tropsch reaction, ChemCatChem 5 (2013) 3384–3397.
[10] J. Cheng, X.Q. Gong, P. Hu, C.M. Lok, P. Ellis, S. French, A quantitative determination of reaction mechanisms from density functional theory calculations: Fischer-Tropsch synthesis on flat and stepped cobalt surfaces, J. Catal. 254 (2008) 285–295.
[11] J. Cheng, P. Hu, P. Ellis, S. French, G. Kelly, C.M. Lok, A DFT study of the chain growth probability in Fischer-Tropsch synthesis, J. Catal. 257 (2008) 221–228.
[12] Y.H. Zhao, K.J. Sun, X.F. Ma, J.X. Liu, D.P. Sun, H.Y. Su, W.X. Li, Carbon chain growth by formyl insertion on rhodium and cobalt catalysts in syngas conversion, Angew. Chem. Int. Ed. 50 (2011) 5335–5338.
[13] R.G. Zhang, L. Kang, H.X. Liu, L.L. He, B.J. Wang, Insight into the C-C chain growth in Fischer-Tropsch synthesis on HCP Co(10-10) surface: the effect of crystal facets on the preferred mechanism, Comput. Mater. Sci. 145 (2018) 263–279.
[14] H.X. Liu, R.G. Zhang, L.X. Ling, Q. Wang, B.J. Wang, D.B. Li, Insight into the preferred formation mechanism of long-chain hydrocarbons in Fischer-Tropsch synthesis on Hcp Co(10-11) surfaces from DFT and microkinetic modeling, Catal. Sci. Technol. 7 (2017) 3758–3776.
[15] C. Masters, The Fischer-Tropsch reaction, Adv. Organomet. Chem. 17 (1979) 61–103.
[16] H. Pichler, H. Schulz, Neuere erkenntnisse auf dem gebiet der synthese von kohlenwasserstoffen aus CO und H2, Chem. Ing. Tech. 42 (1970) 1162–1174.
[17] M.K. Zhuo, K.F. Tan, A. Borgna, M. Saeys, Density functional theory study of the CO insertion mechanism for Fischer-Tropsch synthesis over Co catalysts, J. Phys. Chem. C 113 (2009) 8357–8365.
[18] C.B. Chen, Q. Wang, G.R. Wang, B. Hou, L.T. Jia, D.B. Li, Mechanistic insight into the C2 hydrocarbons formation from syngas on fcc-Co(111) surface: a DFT study, J. Phys. Chem. C 120 (2016) 9132–9147.
[19] X.C. Xu, J.J. Su, P.F. Tian, D.L. Fu, W.W. Dai, W. Mao, W.K. Yuan, J. Xu, Y.F. Han, First-principles study of C2 oxygenates synthesis directly from syngas over CoCu bimetallic catalysts, J. Phys. Chem. C 119 (2015) 216–227.
[20] M. Ojeda, R. Nabar, A.U. Nilekar, A. Ishikawa, M. Mavrikakis, E. Iglesia, CO activation pathways and the mechanism of Fischer–Tropsch synthesis, J. Catal. 272 (2010) 287–297.
[21] G.T.K.K. Gunasooriya, A.P. van Bavel, H.P.C.E. Kuipers, M. Saeys, Key role of surface hydroxyl groups in C–O activation during Fischer–Tropsch synthesis, ACS Catal. 6 (2016) 3660–3664.
[22] Y.Y. Qi, J. Yang, X.Z. Duan, Y.A. Zhu, D. Chen, A. Holmen, Discrimination of the mechanism of methane formation in Fischer-Tropsch synthesis on Co catalysts: a combined approach of DFT, kinetic isotope effects and kinetic analysis, Catal. Sci. Technol. 4 (2014) 3534–3543.
[23] X.Q. Gong, R. Raval, P. Hu, CHx hydrogenation on Co(0001): a density functional theory study, J. Chem. Phys. 122 (2005) 0247111 − 1-6.
[24] A.M.L. Øiestad, E. Uggerud, Gas phase reactivity of small cationic cobalt clusters towards methanol, Chem. Phys. 262 (2000) 169–177.
[25] F. Studt, F.A. Pedersen, Q.X. Wu, A.D. Jensen, B. Temel, J.D. Grunwaldt, J.K. Nørskov, CO hydrogenation to methanol on Cu-Ni catalysts: theory and experiment, J. Catal. 293 (2012) 51–60.
[26] Y.P. Pei, J.X. Liu, Y.H. Zhao, Y.J. Ding, T. Liu, W.D. Dong, J.Z. He, H.X. Su, J.L. Li, W.X. Li, High alcohols synthesis via Fischer-Tropsch reaction at cobalt metal/carbide interface, ACS Catal. 5 (2015) 3620–3624.
[27] J.B. Wang, X.R. Zhang, Q. Sun, Chain growth mechanism on bimetallic surfaces for higher alcohol synthesis from syngas, Catal. Commun. 61 (2015) 57–61.
[28] H. Karaca, O.V. Safonova, S. Chambrey, P. Fongarland, P. Roussel, A. Griboval-Constant, M. Lacroix, A.Y. Khodakov, Structure and catalytic performance of Pt-promoted alumina-supported cobalt catalysts under realistic conditions of Fischer-Tropsch synthesis, J. Catal. 277 (2011) 14–26.
[29] J.X. Liu, H.Y. Su, D.P. Sun, B.Y. Zhang, W.X. Li, Crystallographic dependence of CO activation on cobalt catalysts: HCP versus FCC, J. Am. Chem. Soc. 135 (2013) 16284–16287.
[30] D.I. Enache, B. Rebours, M. Roy-Auberger, R. Revel, In situ, XRD study of the influence of thermal treatment on the characteristics and the catalytic properties of cobalt-based Fischer-Tropsch catalysts, J. Catal. 205 (2002) 346–353.
[31] X.Q. Zhao, S. Veintemillas-Verdaguer, O. Bomati-Miguel, M.P. Morales, H.B. Xu, Thermal history dependence of the crystal structure of Co fine particles, Phys. Rev. B 71 (2005) 024106–1-7.
[32] N.E. Tsakoumis, R. Dehghan, R.E. Johnsen, A. Voronov, W.V. Beek, J.C. Walmsley, Ø. Borg, E. Rytter, D. Chen, M. Rønning, A. Holmen, A combined in situ XAS-XRPD-Raman study of Fischer-Tropsch synthesis over a carbon supported Co catalyst, Catal. Today 205 (2013) 86–93.
[33] A. Tuxen, S. Carenco, M. Chintapalli, C.H. Chuang, C. Escudero, E. Pach, P. Jiang, F. Borondics, B. Beberwyck, A.P. Alivisatos, G. Thornton, W.F. Pong, J.H. Guo, R. Perez, F. Besenbacher, M. Salmeron, Size-dependent dissociation of carbon monoxide on cobalt nanoparticles, J. Am. Chem. Soc. 135 (2013) 2273–2278.
[34] E. Van Steen, M. Claeys, M.E. Dry, J.V. De Loosdrecht, E.L. Viljoen, J.L. Visagie, Stability of nanocrystals: thermodynamic analysis of oxidation and re-reduction of cobalt in water/hydrogen mixtures, J. Phys. Chem. B 109 (2005) 3575–3577.
[35] G.X. Wen, Q. Wang, R.G. Zhang, D.B. Li, B.J. Wang, Insight into the mechanism about the initiation, growth and termination of the C-C chain in syngas conversion on the Co(0001) surface: a theoretical study, J. Phys. Chem. C 18 (2016) 27272–27283.
[36] G. Kresse, J. Furthmüller, Efficient iterative schemes for ab initio total-energy calculations using a plane-wave unit set, Phys. Rev. B 54 (1996) 11169–11186.
[37] G. Kresse, J. Hafner, Ab initio molecular dynamics for open-shell transition metals, Phys. Rev. B 48 (1993) 13115–13118.
[38] J.P. Perdew, J.A. Chevary, S.H. Vosko, K.A. Jackson, M.R. Pederson, D.J. Singh, C. Fiolhais, Erratum: atoms, molecules, solids, and surfaces: applications of the generalized gradient approximation for exchange and correlation, Phys. Rev. B 46 (1992) 6671–6687.
[39] H.J. Monkhorst, J.D. Pack, Special points for brillonin-zone integrations, Phys. Rev. B 13 (1976) 5188–5192.
[40] D. Sheppard, P. Xiao, W. Chemelewski, D.D. Johnson, G. Henkelman, A generalized solid-state nudged elastic band method, J. Chem. Phys. 136 (2012) 074103 − 1-8.
[41] D. Sheppard, R. Terrell, G. Henkelman, Optimization methods for finding minimum

energy paths, J. Chem. Phys. 128 (2008) 134106 – 1-10.
[42] G. Henkelman, H. Jónsson, A dimer method for finding saddle points on high dimensional potential surfaces using only first derivatives, J. Chem. Phys. 111 (1999) 7010–7022.
[43] R.A. Olsen, G.J. Kroes, G. Henkelman, A. Arnaldsson, H. Jónsson, Comparison of methods for finding saddle points without knowledge of the final states, J. Chem. Phys. 121 (2004) 9776–9792.
[44] N.G. Hamilton, R. Warringham, I.P. Silverwood, J. Kapitán, L. Hecht, P.B. Webb, R.P. Tooze, W.Z. Zhou, C.D. Frost, S.F. Parker, D. Lenno, The application of inelastic neutron scattering to investigate CO hydrogenation over an iron Fischer–Tropsch synthesis catalyst, J. Catal. 312 (2014) 221–231.
[45] Y.H. Sun, J.G. Chen, J.G. Wang, L.T. Jia, B. Hou, D.B. Li, J.A. Zhang, The development of cobalt-based catalysts for Fischer-Tropsch synthesis, Chin. J. Catal. 31 (2010) 919–927.
[46] D.R. Lide, CRC Handbook of Chemistry and Physics 4 (1997), pp. 130–136.
[47] B. Liu, W.P. Li, Y.B. Xu, Q. Lin, F. Jiang, X.H. Liu, Insight into the intrinsic active site for selective production of light olefins in cobalt-catalyzed Fischer-Tropsch synthesis, ACS Catal. 9 (2019) 7073–7089.
[48] C. Qin, B. Hou, J.G. Wang, Q. Wang, G. Wang, M.T. Yu, C.B. Chen, L.T. Jia, D.B. Li, Crystal-plane-dependent Fischer – Tropsch performance of cobalt catalysts, ACS Catal. 8 (2018) 9447–9455.
[49] Y.Y. Qi, J. Yang, A. Holmen, D. Chen, Investigation of C1 + C1 coupling reactions in cobalt-catalyzed Fischer-Tropsch synthesis by a combined DFT and kinetic isotope study, Catalysts 9 (2019) 551.
[50] H.Y. Su, Y.H. Zhao, J.X. Liu, K. Sun, W.X. Li, First principles study of structure sensitivity of chain growth and selectivity in Fischer – Tropsch synthesis using HCP cobalt catalysts, Catal. Sci. Technol. 7 (2017) 2967–2977.
[51] R.G. Zhang, F. Liu, Q. Wang, B.J. Wang, D.B. Li, Insight into CHx formation in Fischer–tropsch synthesis on the hexahedron Co catalyst: effect of surface structure on the preferential mechanism and existence form, Appl. Catal. A Gen. 525 (2016) 76–84.
[52] C.J. Weststrate, D. Sharma, D.G. Rodriguez, M.A. Gleeson, H.O.A. Fredriksson, J.W. Niemantsverdriet, Mechanistic insight into carbon-carbon bond formation on cobalt under simulated Fischer-Tropsch synthesis conditions, Nat. Commun. 750 (2020) 11.
[53] L. Barrio, P. Liu, J.A. Rodriguez, J.M. Compos-Martin, J.L.G. Fierro, Effects of hydrogen on the reactivity of O2 toward gold nanoparticles and surfaces, J. Chem. Phys. 111 (2007) 19001–19008.
[54] R.A. Van Santen, A.J. Markvoort, I.A.W. Filot, M.M. Ghouri, E.J.M. Hensen, Mechanism and microkinetics of the Fischer-Tropsch reaction, Phys. Chem. Chem. Phys. 15 (2013) 17038–17063.
[55] Y.M. Choi, P. Liu, Mechanism of ethanol synthesis from syngas on Rh(111), J. Am. Chem. Soc. 131 (2009) 13054–13061.
[56] N.Y. Yang, A.J. Medford, X. Liu, F. Studt, T. Bligaard, S.F. Bent, J.K. Nørskov, Intrinsic selectivity and structure sensitivity of rhodium catalysts for C(2 +) oxygenate production, J. Am. Chem. Soc. 138 (2016) 3705–3714.
[57] I.A.W. Filot, R.J.P. Broos, J.P.M. van Rijn, G.J.H.A. van Heugten, R.A. van Santen, E.J.M. Hensen, First-principles-based microkinetics simulations of synthesis gas conversion on a stepped rhodium surface, ACS Catal. 5 (2015) 5453–5467.
[58] R.A. van Santen, M.M. Ghouri, E.J.M. Hensen, Microkinetics of oxygenate formation in the Fischer – Tropsch reaction, Phys. Chem. Chem. Phys. 16 (2014) 10041–10058.
[59] I.A.W. Filot, B. Zijlstra, R.J.P. Broos, W. Chen, R. Pestman, E.J.M. Hensen, Kinetic aspects of chain growth in Fischer – Tropsch synthesis, Faraday Discuss. 197 (2017) 153–164.
[60] R.A. van Santen, A.J. Markvoort, M.M. Ghouri, P.A.J. Hilbers, E.J.M. Hensen, Monomer formation model versus chain growth model of the Fischer-Tropsch reaction, J. Phys. Chem. C 117 (2013) 4488–4504.
[61] I.A.W. Filot, R.A. van Santen, E.J.M. Hensen, The optimally performing Fischer-Tropsch catalyst, Angew. Chem., Int. Ed. 53 (2014) 12746–12750.
[62] A.C. Lausche, A.J. Medford, T.S. Khan, Y. Xu, T. Bligaard, F. Abild-Pedersen, J.K. Nørskov, F. Studt, On the effect of coverage dependent adsorbate – adsorbate interactions for CO methanation on transition metal surfaces, J. Catal. 307 (2013) 275–282.
[63] Z.H. Yao, C.X. Guo, Y. Mao, P. Hu, Quantitative determination of C – C coupling mechanisms and detailed analyses on the activity and selectivity for Fischer-Tropsch synthesis on Co(0001): microkinetic modeling with coverage effects, ACS Catal. 9 (2019) 5957–5973.
[64] S.H. Zeng, Y. Du, H.Q. Su, Y.L. Zhang, Promotion effect of single or mixed rare earths on cobalt-based catalysts for Fischer–Tropsch synthesis, Catal. Commun. 13 (2011) 6–9.
[65] B. Qiu, C. Yang, W.H. Guo, Y. Xu, Z.B. Liang, D. Ma, R.Q. Zou, Highly dispersed Co-based Fischer-Tropsch synthesis catalysts from metal-organic frameworks, J. Mater. Chem. A Mater. Energy Sustain. 5 (2017) 8081–8086.
[66] S. Lyu, L. Wang, J.H. Zhang, C. Liu, J.M. Sun, B. Peng, Y. Wang, K.G. Rappé, Y.H. Zhang, J.L. Li, L. Nie, Role of active phase in Fischer – Tropsch synthesis: experimental evidence of CO activation over single-phase cobalt catalysts, ACS Catal. 8 (2018) 7787–7798.
[67] M.A. Petersen, J.A. van den Berg, I.M. Ciobîcă, P. van Helden, Revisiting CO activation on Co catalysts: impact of step and kink sites from DFT, ACS Catal. 7 (2017) 1984–1992.
[68] O.R. Inderwildi, S.J. Jenkins, D.A. King, Fischer-Tropsch mechanism revisited: alternative pathways for the production of higher hydrocarbons from synthesis gas, J. Phys. Chem. C 112 (2008) 1305–1307.
[69] N. Fischer, E.V. Steen, M. Claeys, Preparation of supported nano-sized cobalt oxide and fcc cobalt crystallites, Catal. Today 171 (2011) 174–179.
[70] T.O. Eschemann, W.S. Lamme, R.L. Manchester, T.E. Parmentier, A. Cognigni, M. Rønning, K.P. De Jong, Effect of support surface treatment on the synthesis, structure, and performance of Co/CNT Fischer-Tropsch catalysts, J. Catal. 328 (2015) 130–138.
[71] F.T. Kong, X. Jing, C. Jie, A. Borgna, M. Saeys, Carbon deposition on Co catalysts during Fischer-Tropsch synthesis: a computational and experimental study, J. Catal. 274 (2010) 121–129.
[72] M.K. Gnanamani, G. Jacobs, W.D. Shafer, B.H. Davis, Fischer–tropsch synthesis: activity of metallic phases of cobalt supported on silica, Catal. Today 215 (2013) 13–17.